CRREL
REPORT 88-21

DTIC
S FEB 2 8 1989 **D**
C&D

AD-A205 010

Measurement of frost heave forces on H-piles and pipe piles

THERMAL SIPHON RADIATORS

GRAVEL LAYER

ICE COLLARS

GROUND SURFACE

OCT 31
NOV 30
DEC 31
JAN 25

ACTIVE LAYER

TOP OF PERMAFROST

H-PILE

PIPE PILE

ANTI HEAVE ANCHOR PLATES RINGS

008

CRREL Report 88-21

December 1988

Measurement of frost heave forces on H-piles and pipe piles

Jerome B. Johnson and James S. Buska

REPORT DOCUMENTATION PAGE

Form Approved
OMB NO. 0704-0188
Exp. Date: Jun 30, 1986

1a. REPORT SECURITY CLASSIFICATION Unclassified	1B. RESTRICTIVE MARKINGS
2a. SECURITY CLASSIFICATION AUTHORITY	3. DISTRIBUTION/AVAILABILITY OF REPORT
2b. DECLASSIFICATION/DOWNGRADING SCHEDULE	Approved for public release; distribution is unlimited.

4. PERFORMING ORGANIZATION REPORT NUMBER(S) CRREL Report 88-21	5. MONITORING ORGANIZATION REPORT NUMBER(S)

6a. NAME OF PERFORMING ORGANIZATION U.S. Army Cold Regions Research and Engineering Laboratory	6b. OFFICE SYMBOL (If applicable) CECRL	7a. NAME OF MONITORING ORGANIZATION State of Alaska Department of Transportation and Public Facilities

6c. ADDRESS (City, State, and ZIP Code) 72 Lyme Road Hanover, New Hampshire 03755-1290	7b. ADDRESS (City, State, and ZIP Code) Divison of Planning and Programming Research Section Fairbanks, Alaska 99701

8a. NAME OF FUNDING/SPONSORING ORGANIZATION	8b. OFFICE SYMBOL (If applicable)	9. PROCUREMENT INSTRUMENT IDENTIFICATION NUMBER HPR-84-12

| 8c. ADDRESS (City, State, and ZIP Code) | 10. SOURCE OF FUNDING NUMBERS |

PROGRAM ELEMENT NO.	PROJECT NO.	TASK NO.	WORK UNIT ACCESSION NO.

11. TITLE (Include Security Classification)

Measurement of Frost Heave Forces on H-Piles and Pipe Piles

12. PERSONAL AUTHOR(S)
Johnson, Jerome B. and Buska, James S.

13a. TYPE OF REPORT	13b. TIME COVERED FROM _____ TO _____	14. DATE OF REPORT (Year, Month, Day) December 1988	15. PAGE COUNT 58

16. SUPPLEMENTARY NOTATION

Additional funding by Federal Highway Administration

17. COSATI CODES			18. SUBJECT TERMS (Continue on reverse if necessary and identify by block number)
FIELD	GROUP	SUB-GROUP	

19. ABSTRACT (Continue on reverse if necessary and identify by block number)

The magnitude and variation of forces and shear stresses, caused by frost heaving in Fairbanks silt and the adfreeze effects of a surface ice layer and a gravel layer, were determined as a function of depth by using electric strain gauges along the upper 2.75 m of a pipe pile, 30.5-cm I.D. x 0.95-cm wall, and an H-pile, 25.4-cm web x 85 kg/lineal m. The peak frost heaving forces on the H-pile for three consecutive winter seasons (1982–1985) were 752, 790 and 802 kN, respectively. Peak frost heaving forces on the pipe pile of 1118 and 1115 kN were determined only for the second and third winter seasons. Maximum average shear stresses acting on the H-pile were 256, 348 and 308 kPa during the three winter seasons. Maximum average shear stresses acting on the pipe pile were 627 and 972 kPa for the second and third winter seasons. Ice collars were placed around the tops of both piles during the first and third winter seasons to measure the adfreeze effects of a surface ice layer. The ice layer may have contributed 15 to 20% of the peak forces measured on the piles. A 0.6-m-thick gravel layer replaced the soil around the tops of both piles for the second and third winter seasons to measure the adfreeze effects of a gravel backfill. The gravel layer on the H-pile may have contributed about 35% of the peak forces measured. Maximum heaving forces and shear stresses occurred during periods of maximum cold and soil surface heave magnitude. These were not related to the depth of frost penetration for most of the winter since frost was present at all depths extending to the permafrost table. Soil surface dis-

20. DISTRIBUTION/AVAILABILITY OF ABSTRACT ☒ UNCLASSIFIED/UNLIMITED ☐ SAME AS RPT. ☐ DTIC USERS	21. ABSTRACT SECURITY CLASSIFICATION Unclassified	
22a. NAME OF RESPONSIBLE INDIVIDUAL James S. Buska	22b. TELEPHONE (Include Area Code) 603-646-4100	22c. OFFICE SYMBOL CECRL-EC

19. Abstract (cont'd).

placements of 2 to 7 cm were measured at the experiment site during the study. The important mechanisms that determine the magnitude of uplift heave forces are 1) soil heaving as the driving force, and 2) soil temperature, which controls the unfrozen water content, mechanical properties of the soil and the area of influence of heaving pressure.

PREFACE

The contents of this report are not to be used for advertising or promotional purposes. Citation of brand names does not constitute an official endorsement or approval of the use of such commercial products.

Accesion For		
NTIS CRA&I		✓
DTIC TAB		☐
Unannounced		☐
Justification		
By		
Distribution /		
Availability Codes		
Dist	Avail and / or Special	
A-1		

iii

CONTENTS

ILLUSTRATIONS

TABLES

CONVERSION FACTORS: METRIC (SI) TO U.S. CUSTOMARY UNITS OF MEASUREMENT

These conversion factors include all the significant digits given in the conversion tables in the ASTM *Metric Practice Guide* (E 380), which has been approved for use by the Department of Defense. Converted values should be rounded to have the same precision as the original (see E 380).

Multiply	By	To obtain
centimeter	0.39371	inch
meter	3.280840	foot
meter^2	10.763910	foot^2
kilogram	2.204624	pound
kilonewton	0.224809	kip
kilopascal	0.145038	psi

Measurement of Frost Heave Forces on H-piles and Pipe Piles

JEROME B. JOHNSON AND JAMES S. BUSKA

INTRODUCTION

Foundations embedded in frost-susceptible soils can be subjected to large uplift forces resulting from frost heaving of the soils. These forces can cause an upward vertical displacement of foundations that are not embedded below the frost depth or do not have sufficient resistance to counteract heaving forces. In Alaska, H- and pipe piles are often used to support buildings, bridges and dock structures. It is important that design engineers know the magnitude of frost heaving forces that can act on foundation piles and how these forces are distributed along the piles. This information is used to determine the depth to which a pile needs to be embedded, how it must be loaded to resist heaving forces, and the tensile strength requirements of the pile.

This report presents the results of a three-year study designed to measure and record the magnitude and distribution of axial strains, as a function of depth, time and temperature, for an H-pile and a pipe pile penetrating surficial layers of ice and gravel and embedded in Fairbanks silt with an active layer overlying permafrost. We used the measured strains to calculate the uplift forces acting on the piles and the shear stresses at the soil/pile interface. Soil temperatures and surface heave were also measured. These results provided complete force and stress information on the piles as they were subjected to annual cycles of frost heaving and thaw consolidation. In general, previous studies have provided data on only the total frost heaving load acting on pipe piles (Crory and Reed 1965, Penner and Irwin 1969, Penner 1974).

SUMMARY OF PREVIOUS RESEARCH

Studies of the uplift forces induced by frost heaving of foundations date back to early Soviet work in the 1930s reported by Tsytovich (1975).

Direct measurements of frost heave forces were made in the U.S.S.R. from 1958-1963. Three types of instrumentation were used to measure frost heave forces: 1) reaction beam and load cell, 2) force balance apparatus, and 3) electric strain gauges. The reaction beam device consisted of a beam held in place with rods anchored into the soil at depth. The test pile was restrained from moving by the reaction beam, and the uplift forces acting on the pipe were measured with a load cell placed between the beam and pile. In the force balance scheme, an additional load compensated for any vertical displacement of the test pile. The load that just completely stopped the heaving of the pile during the freezing of the soil was taken as the maximum total heave force.

Additional frost heave measurements were made using electric strain gauges mounted on the inner surface of a tubular pile. The results of the experiment, reported by Tsytovich (1975), were presented in terms of kilograms-force per lineal centimeter of column perimeter. This is equivalent to the shear stress (kgf/cm²) times a unit depth of 1.0 cm. Since the pile diameter was not given, the actual shear stress values cannot be determined. The results can, however, be used to examine how the shear stress varies along the depth of the pile. Figure 1 shows the force per lineal centimeter of column perimeter (shear stress times a unit depth of 1.0 cm) acting on the pile with respect to depth. Shear stresses acting on the pile were zero at the soil surface, then reached a maximum at some depth between the soil surface and the 0°C isotherm, and finally decreased to zero near the 0°C isotherm. The maximum of the shear stresses shifted downward toward the freezing boundary as the frost depth increased. Shear stresses acting along the soil/pile interface increased along the pile length with time and decreasing soil temperature (Tsytovich 1975). The results for the strain-gauged pipe are of interest because of the similarity to the test setup in this study. They indicate
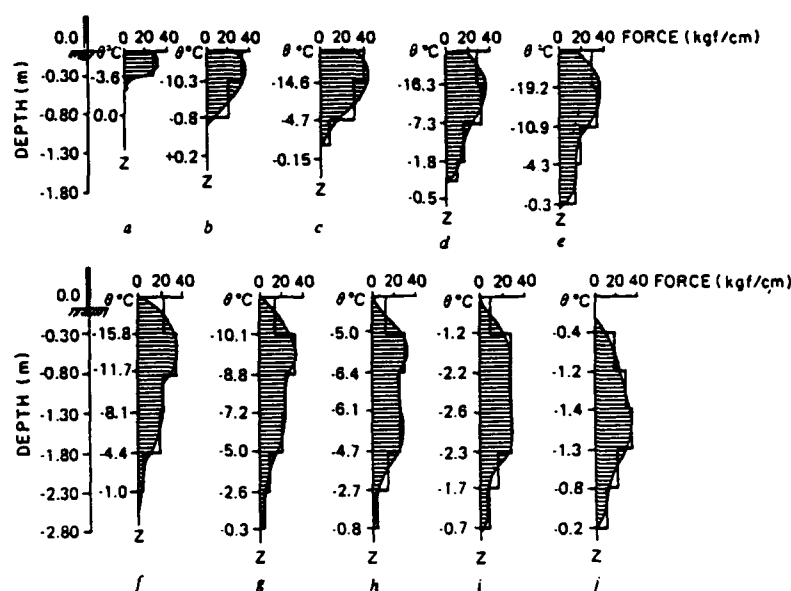
Figure 1. Distribution of relative frost-heaving forces, in kilograms-force per lineal centimeter of column perimeter, over the lateral surface of the pile (experiments of Yegerev reported by Tsytovich 1975). z is depth in meters from the surface and θ is the temperature in degrees Celsius.

a—4 Nov 1957.	f—11 Mar 1958.
b—14 Nov 1957.	g—16 Apr 1958.
c—25 Nov 1957.	h—5 May 1958.
d—28 Dec 1957.	i—26 May 1958.
e—11 Jan 1958.	j—11 Jun 1958.

that the shear stresses (due to frost heaving) are not uniform along the length of the pile. There is not sufficient information about the setup or procedures used in the Soviet experiment to allow an accurate comparison to other available experimental results.

Additional field measurements of frost heaving forces on piles have been conducted in Japan, the United States and Canada (Kinosita and Ono 1963, Crory and Reed 1965, Penner and Irwin 1969, Penner and Gold 1971, Penner 1974, Domaschuk 1982).. These have consisted of reaction beam and load cell tests. Crory and Reed (1965) conducted an experiment using a strain-gauged pile; however, the results of the test were not published. They reported the results of frost heaving force measurements conducted from 1956 to 1963 on 203-mm standard steel pipe and 330- and 381-mm butt diameter creosoted timber piles. The piles were embedded in silty soils overlying permafrost at the CRREL Alaska Field Station in Fairbanks. The site conditions were very similar to those of the current study, which was also located at the field station. Air temperature, soil temperature,

heaving of an unrestrained pile, heaving of the test pile and the heave force were measured during the winters of 1956-1957, 1957-1958 and 1962-1963. The forces observed in the first two tests (1956-1957 and 1957-1958) were lower than the maximum forces that might have been generated because the adfreeze bond between the reaction beam support piles and permafrost was not sufficient to resist heaving during the 1956-1957 test and the soil was exceptionally dry during the 1957-1958 test. Distinct fluctuations in the heave force measurements were observed for both steel and timber piles. The maximums and minimums of the fluctuations occurred a few days after a respective decrease or increase in air and soil temperatures (Crory and Reed 1965).

Canadian experiments measured heaving forces of wood, steel and concrete columns, from 76 mm to 305 mm in diameter, embedded in Leda clay (Penner and Irwin 1969, Penner and Gold 1971, Penner 1974). The shear stresses from heaving were highest for steel, followed by concrete and wood. This was mostly attributed to the influence of temperature on the adfreeze strength of frozen

Table 1. Maximum average uplift shear stresses measured on steel, concrete and wood piles.

Soil type	Year of test	Pile diameter (mm)	Shear stress (kPa)				Investigators
			Steel	Vinyl	Concrete	Wood	
Silty clay	1961–62	72	207				Kinosita and Ono (1983)
		76		162	114 (uncoated)		
	1061–62	94			51 (resin coated)		
Silt	1956–57	203	152				Crory and Reed (1965)
	1957–58	203	159				
	1958–59	356				55	
	1962–63	356				83	
	1962–63	203	283				
?	1958–63	?				97–165	Soviet data reported by Tsytovich (1975)
Clay	1966–67	89	83				Penner and Irwin (1969)
	1967–68	89	83				
Clay	1970	89	114		134	90	Penner and Gold (1971)
Clay	1970–71	76			114	116	Penner (1974)
	1970–71	156			150	177	
	1970–71	305			119	139	
	1971–72	76	255		192	131	
	1971–72	152	203		249	226	
	1971–72	305	172		141	243	
Silt		76×76 angle	345				Domaschuk (1982)
Clay with frozen gravel surface layer, Thompson, Manitoba	1972–73	169	379	(loads exceeded cell capacity)			Penner and Goodrich (1983)
		323	179				
		458	124				
	1973–74	169	117				
		323	76				
		458	69				
	1974–75	169	69				
		323	55				
		458	48				
Clay, Ottawa, Ontario	1971–72	169	93				
		323	70				

soil acting on the columns. The steel columns were normally colder than the concrete or wood columns. Domaschuk (1982) conducted controlled tests on embedded vertical steel members and steel members inclined to the soil surface. The test results indicated a decrease in vertical stress as the angle of inclination of the member with respect to the frost plane increased. Kinosita and Ono (1963) conducted frost heave force measurement tests on steel, concrete, resin-coated concrete and vinyl columns. These tests indicated that adfreeze strength was the greatest for steel and was lower for vinyl and wood. The Canadian and Japanese experiments both showed the fluctuations in heave force associated with changes in the air temperature that had been observed by Crory and Reed (1965). These were attributed to changes in ground temperature and ground temperature gradients caused by air temperature fluctuations. Table 1 summarizes the measurements of maximum averaged uplift shear stress acting along the soil/pile interface. The uplift shear stress is induced by frost heaving and computed on the basis of the uplift force divided by the surface area of the pile from the soil surface to the depth of the 0°C isotherm.

An inherent problem with the reaction beam and force-balance methods is that they may under-

estimate the uplift shear stresses by not taking into account the resistive shear stresses on piles. The heaving forces measured in these tests are used to estimate an average uplift shear stress which acts on the pile from the soil surface to the depth of the 0°C isotherm. No allowance is made for resistive shear stresses developed on the pile in the soil below the 0°C isotherm. Therefore, the reaction beam and force-balance methods actually measure a net uplift force, which is the total uplift load less the total restraining load acting on the pile.

Johnson and Esch (1985) reported on the 1982–83 and 1983–84 winter seasons from this study using the initial calibration results. The magnitude and distribution of strains, forces and stresses differ slightly from the results of this report because of differences in the calibration results used for the reports. Figure 2 shows the maximum measured adfreeze shear stresses for the H-pile as a function of temperature from October 1983 through March 1984 (Johnson and Esch 1985). Their results indicated that the apparent relationship between adfreeze stress and temperature also depended on the rate and magnitude of soil heave and that it was not possible to completely separate the effects of soil heave and temperature on shear stresses.

The above investigators suggested a number of controlling influences for frost heaving forces acting on foundation piles. These included 1) soil type and temperature, 2) rate and magnitude of

Figure 2. Shear stress as a function of temperature for the H-pile from October 1983 through March 1984 (from Johnson and Esch 1985).

soil surface heave, 3) changes in soil temperature, 4) soil temperature gradients and 5) the availability of moisture in the soil. Maximum shear stresses generally occurred during the early freezing period when heaving rates were high. Maximum uplift forces often occurred near the time of maximum frost penetration.

METHODS AND MATERIALS

Soil conditions

The test site was located at the CRREL Field Station in Fairbanks (Fig. 3). The soils (Fairbanks silt) are primarily deep colluvial deposits of slightly organic silts with occasional wood fragments and peat layers (Crory and Reed 1965, Linell 1973, Esch 1982). Moisture content was not measured in the fall preceding the 1982–83 measurement program; however, observation of the borehole cuttings and other evidence indicated that the soil deposits were saturated below a depth of about 0.5 m. A soil log taken prior to the 1983–84 winter indicated the moisture content of the soil was 40% near the surface and varied from 25% to 29% between the surface and a depth of about 2.4 m. Prior to the beginning of the 1982–83 winter season, the soil was unfrozen to a depth of about 2.5 m with permafrost below. Measurements of the depth to permafrost in September 1984 indicated that the depth of unfrozen ground was approximately 2.5 m where the ground was snow-covered during the winter, 1.6 m between the piles, and 2 m immediately adjacent to the piles. These measurements indicated that the top of the permafrost table had moved toward the surface of the experiment site as a result of maintaining a snow-free surface to intensify frost heaving. The thickness of the seasonally thawed or active layer between the piles at the beginning of the winter season was 2.3 m in 1982, 1.6 m in 1983 and 1.6 m in 1984. The soil in the active layer froze to the depth of the permafrost each winter during the study as illustrated in Figure 4. During a typical winter, frost heaving at the site ranges from 2 to 7 cm.

Site preparation and plan

The experiment site had been cleared of vegetation and covered with a 30-cm layer of gravel during an earlier study designed to investigate methods for pre-thawing permafrost. The location of the pile study site was previously designated as "plot D," and the average thaw depth was measured at 2.5 m in the fall of 1982 (Esch 1983). Most
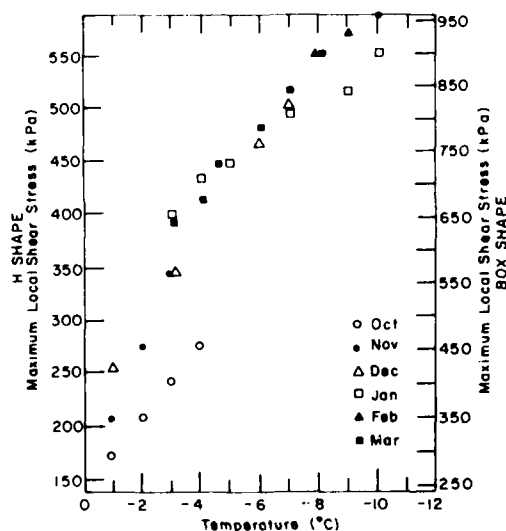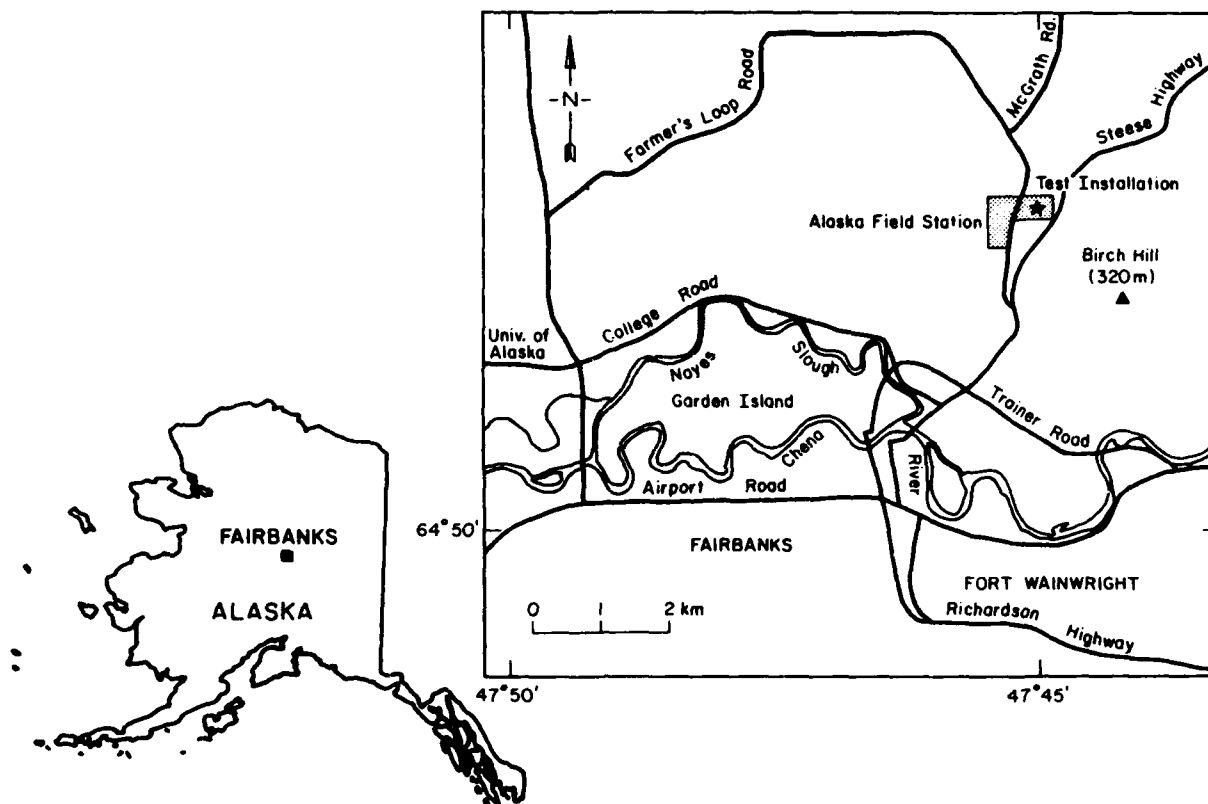
4

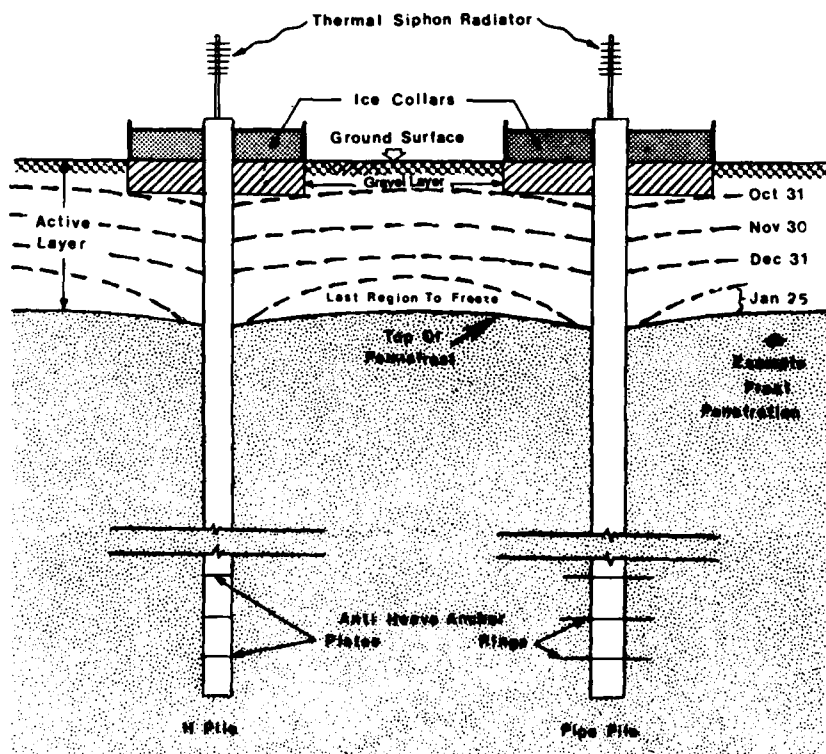Figure 3. Experiment site location map.

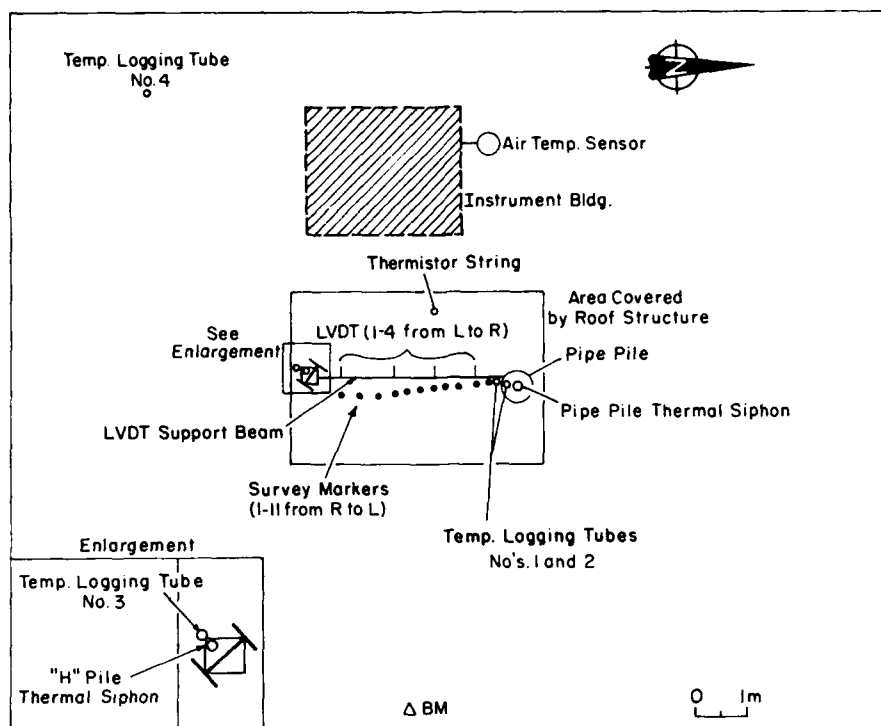Figure 4. Development of frost penetration at the experiment site.

Figure 5. Plan view of the experimental site.

of the 30-cm layer of gravel was removed during site preparation, leaving a thin layer of gravel. Two instrumented piles, a pipe pile and an H-pile, were installed at the test site for this study. A reference benchmark, temperature probes, and an instrumentation hut were also installed (Fig. 5).

The ground around the piles was kept free of snow throughout the measurement program. A roof structure was installed over the piles for the 1983–84 and 1984–85 seasons to keep the snow off the site and thereby increase the frost penetration and intensify frost heave.

Two commonly encountered situations for pile installations in Alaska are aufeis buildup around piles near river crossings and the use of gravel backfill around the top of piles. The experimental configuration was designed to allow for surficial ice buildup and the use of gravel backfill. Ice collars 1.8 m in diameter were installed around the upper sections of the piles during the 1982–83 and 1984–85 seasons in an effort to measure the adfreeze effects of surface ice deposits in pilejacking. The ice collars for the 1982–83 season were placed between 5 and 13 January 1983 to a thickness of 25 cm. The ice collars for the 1984–85 season were placed between 16 and 20 November 1984 to a thickness of 45 cm. Ice collars were not used dur-

ing the 1983–84 season. A 0.6-m-thick × 1.8-m-diameter gravel layer was placed around the tops of the piles on 17–23 August 1983 prior to the 1983–84 winter season and left in place throughout the 1984–85 season. The gravel layer was placed by excavating the soil from around the tops of the piles and backfilling with gravel to the original ground surface.

Instrumentation and installation of piles

An H-pile, 25.4-cm web × 85 kg/lineal meter (HP 10×57), and a pipe pile 30.5-cm I.D. × 0.95-cm wall thickness, were each instrumented with hermetically sealed weldable strain gauges (HITEC Corp., 350-ohm strain gauges) and copper-constantan thermocouples. These were placed every 15.2 cm along the upper 3 m of the 9.45-m length of both piles as shown in Figure 6. The gauges were mounted along the centerline on both sides of the web for the H-pile and on diametrically opposite sides of the pipe pile. Strain gauges oriented at 90° to the axial direction were interspersed between the axially oriented gauges along the length of the instrumented sections. These were used to measure transverse strains in the piles and to estimate the magnitude of horizontal compressive stresses in the soil acting on the piles. Temperature-
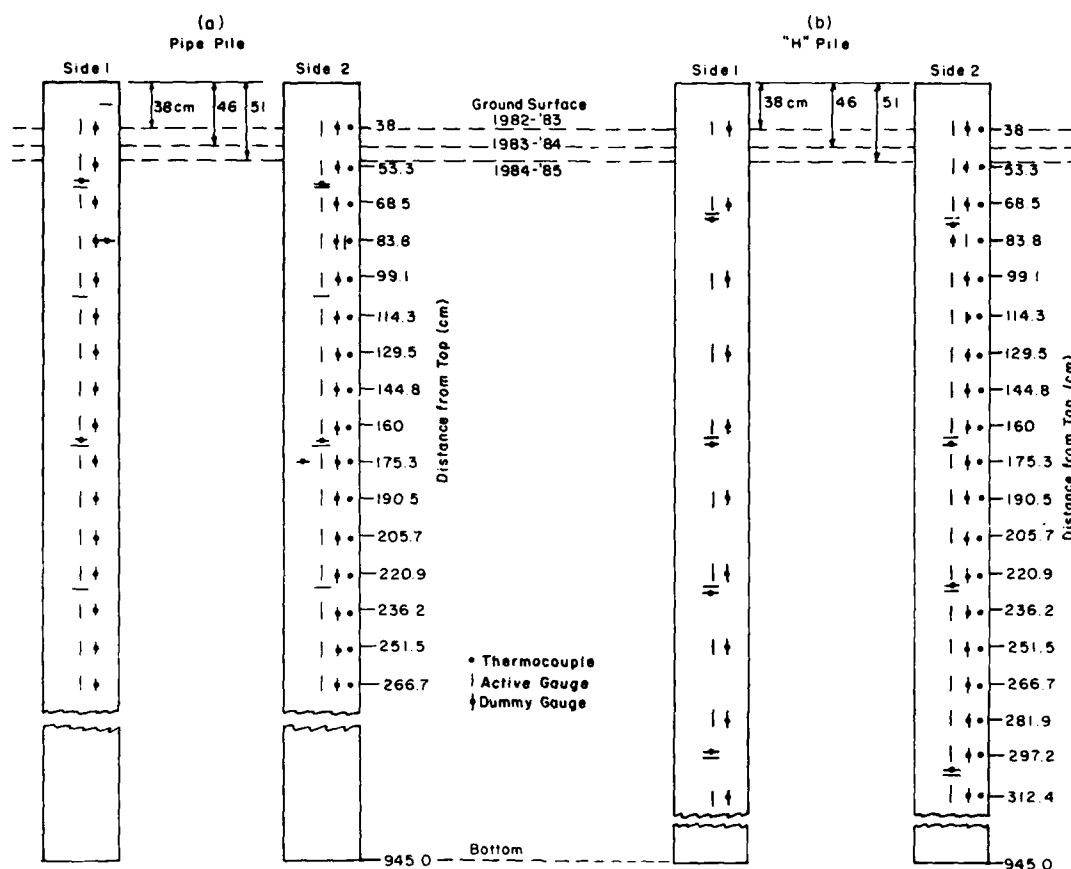
6

Figure 6. Strain and thermocouple installation layout for the pipe pile (a) and the H-pile (b).

induced apparent strains were measured using strain gauges mounted on thin metal plates with the same thermal expansion properties as the piles, with one end fixed to the pile to ensure that the gauge–shim system was unstressed (shown as dummy gauges in Fig. 6). Dummy gauges were wired to active gauges to cancel temperature-induced apparent strain (shown as pairs of gauges in Fig. 6). The gauges were coated with a water-proof coating and polyurethane foam to provide corrosion protection and insulation.

Angle sections (L5 × 5 × ¾, 12.7-cm legs, 0.95 cm thick) were welded over the gauges on each side of the H-pile web to provide mechanical protection. Figure 7 shows the installation scheme for two axially oriented and one transverse strain gauge with a thermocouple installed next to each of the axial gauges on the H-pile. A 3.35-m-long tube was placed inside the angle on one side of the pile and connected to a watertight box section (4 × 4 × ¼, 10.2-cm sides, 0.64 cm thick), which extended the remaining length of the H-pile. The tube and box section were used as a guide and

housing for a thermal siphon. Polyurethane foam was used to fill the cavity inside the angle sections for the length of the instrumented pile section. Frost heave resistance was obtained through steel plates welded between the flanges of the H-pile at 0.3-m intervals over the bottom 3.0 m of the pile (Fig. 8).

The upper 2.74 m of the pipe pile was cut into three 0.91-m sections to facilitate placement of instrumentation on the pile (Fig. 9). After instrumentation placement, these pile sections were welded together, calibrated and then welded to the lower uninstrumented section of the pipe pile. The gauges were kept cool during welding by blowing a stream of air through the pile and running water over the outer skin. Concentric rings with a 40.6-cm outer diameter were welded to the lower 3.0-m section of the pipe pile at 0.3-m intervals to help prevent the pile ⸰⸰om heaving throughout the winter period.

Two tubes were placed in the interior of the pipe pile. One tube was suspended in the center of the pile as a guide for a thermal siphon. The second

7

Figure 7. Closeup of axial and transverse strain gauge and thermocouple installations on the H-pile.

Figure 8. Instrumented H-pile after installation of protective angles, guide tube and retention bars.

Figure 9. End view of 0.91-m-long pipe pile section instrumented with strain gauges and thermocouples.

Figure 10. Instrumented pipe pile after welding of the three instrumented sections to the uninstrumented section and installation of the polyurethane foam.

tube was slightly offset from the center and was used to pour a slurry of water and sand in the uninstrumented portion of the pipe pile after installation to provide for better thermal conduction between the thermal siphon and the pipe walls. Once both tubes were in place, polyurethane foam was used to fill the upper 2.75-m cavity of the pile (Fig. 10).

Both the H- and pipe piles were calibrated in compression prior to installation and in tension at the end of the experiment. A description of the initial (compression) and field (tension) calibration procedures is given in Appendix B.

After the initial calibration the piles were installed in holes augered to a depth of approximately 9 m. The holes around the piles were backfilled during the week of 31 October 1982 with a saturated sand slurry mixture for the lower 6 m and with native silt at 40% water content by weight for the upper 3 m. Thermal siphon tubes with propane as the refrigerating fluid were installed in both piles to aid in freezing the backfill slurry and cooling the permafrost, thereby increasing the frost jacking resistance of the piles in combination with the rings and plates welded on for the same purpose. The polyurethane foam surrounding the upper third of the thermal siphons in both piles helped reduce air cooling of the piles and radial freezing of the soil, which might have altered soil temperatures and reduced heave stresses. Three temperature logging tubes, consisting of 2.54-in. PVC tubing filled with diesel fuel, were installed at the locations shown in Figure 5 to a depth of 9 m around the piles to monitor the effectiveness of the thermal siphons. Temperature readings were taken in the logging tubes near the piles and at an adjacent undisturbed soil site on two different occasions. Tube 1 was located inside the pipe pile about 6.4 cm from the thermal siphon, and tube 2 was located 25.4 cm outside the pipe pile. Tube 3 was located about 29 cm from the H-pile thermal siphon and tube 4 was located 3.1 m from the H-pile (Fig. 5). Figure 11 shows that the soil at depth immediately surrounding the pipe pile was about 2° to 4°C cooler than the undisturbed soil on 7 December 1982 and continued to cool throughout the winter. Figure 12 shows that the soil around the H-pile at depth was about 0.5° to 3°C cooler than the undisturbed soil. The effectiveness of the thermal siphon for the H-pile was less than that used in the pipe pile, possibly because of differences in thermal contact between the piles and their thermal siphons.

9
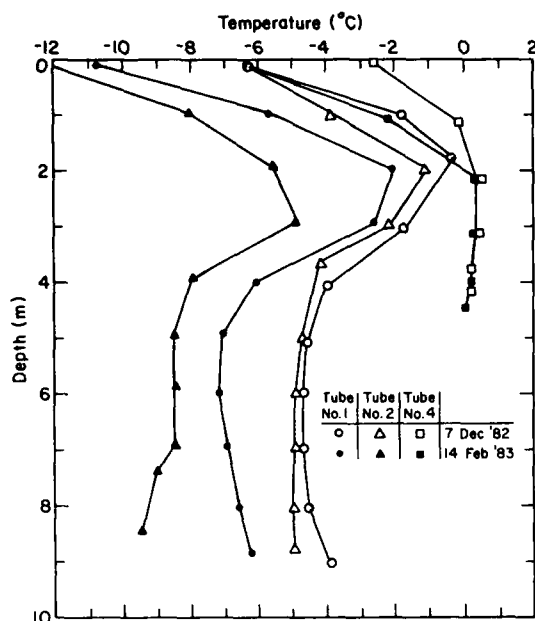
Figure 11. Temperature profiles in the vicinity of the pipe pile and in undisturbed soil. Tube 1 was located inside the pipe 6.4 cm from the thermal siphon, tube 2 was located about 25.4 cm from the thermal siphon, and tube 4 was located about 3.1 m from the experimental site.

Figure 12. Soil temperature profile near the H-pile. Tube 3 was about 29.2 cm from the thermal siphon and tube 4, in undisturbed soil, was about 3.1 m from the experimental site.

Temperature measurements

Temperatures for the soil, piles and air were recorded throughout the study. Copper-constantan thermocouples were installed at 15.2-cm intervals on each pile. An air temperature sensor was mounted in a protective housing on the north side of the instrumentation hut. Soil temperatures were measured at the location of the thermistor string in Figure 5 using thermistors placed every 15.2 cm to a depth of 2.75 m.

Soil surface heave measurements

Standard level survey practices were used during the 1982–83 season to determine changes in elevation of the piles and of several intermediate survey markers between the piles as shown in Figure 5. These observations were made monthly, with differences in elevation between surveys being determined to an accuracy of 1 mm. Survey markers 1, 2, 10 and 11 were covered with ice on 10 January 1983 to create an ice layer around the tops of the piles. The vertical displacements for markers 3 through 9 were used to determine the average incremental and accumulated vertical displacements for the soil surface for the 1982–83 season (Fig. 13). Figure 13 also shows the survey results for the

Figure 13. Average incremental and accumulated soil surface vertical heave and incremental vertical displacement for the H- and pipe piles.

10

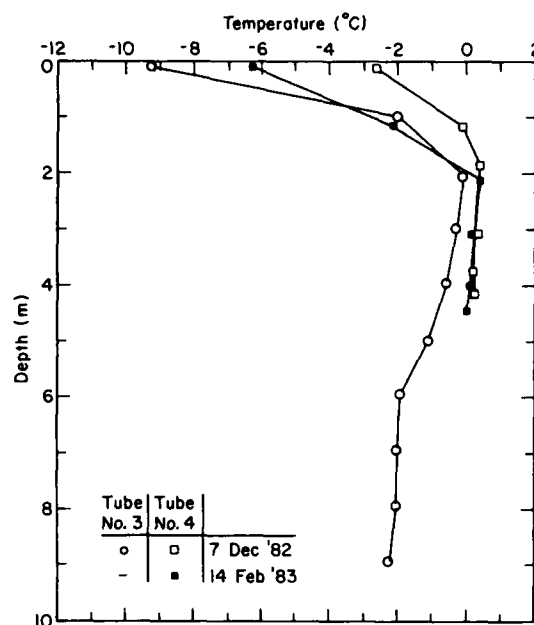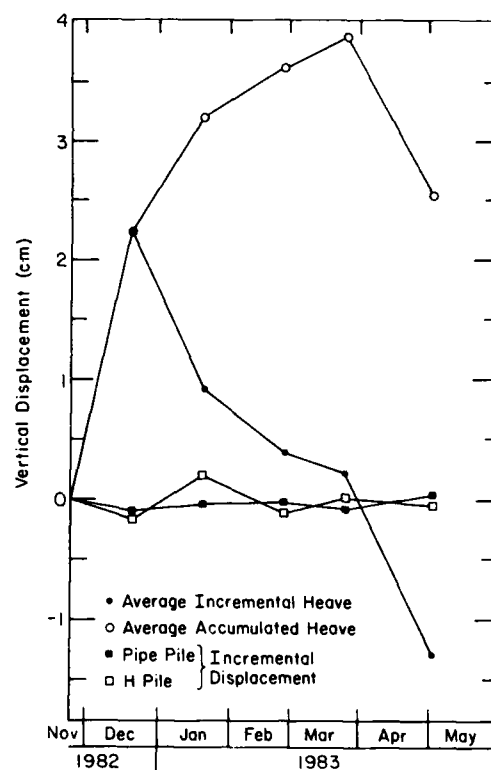H- and pipe piles during the winter season. The survey measurements indicated that the piles did not change elevation during the 1982–83 season. Therefore, linear variable displacement transformers (LVDTs) mounted on a beam suspended between the piles were used to measure the ground surface heave during the 1983–84 and 1984–85 seasons. The LVDTs were located along the beam at distances of 0.3 and 1.2 m from the H-pile and 0.4 and 1.2 m from the pipe pile for the 1983–84 season, and at distances of 0.3 and 0.9 m from both the H-pile and pipe pile for the 1984–85 season (Fig. 5). A reference elevation was established at the top of the pipe pile and the ground level elevation determined from the reference elevation for each year of the study. The ground surface was 0.38, 0.46 and 0.51 m below the top of the pipe pile for the 1982–83, 1983–84 and 1984–85 winter seasons, respectively, as a result of thaw consolidation and the disturbances caused by placing a gravel layer and ice collars around the tops of the piles (Fig. 6). The vertical displacements measured are relative to the time that heave measurements started each season. Vertical displacements of the soil surface prior to the beginning of displacement measurements are considered to be minimal.

Force and shear stress calculations

The magnitude of frost-heave-induced shear stress along the soil/pile interface was determined by using resistance strain gauge measurements to calculate the internal axial stresses in the piles (App. A). We then used these stresses to calculate the internal axial forces in the piles at the gauge locations. The frost-heave-induced shear stresses along the soil/pile interface were then calculated by dividing the difference in force between two adjacent strain gauges by the corresponding pile surface area.

Internal axial stresses on both the H-pile and pipe piles can be determined from

$$\sigma'_z = E \epsilon'_z \qquad (1)$$

where σ'_z = the internal axial stress in the pile
E = Young's modulus determined from the field calibration test results (App. B)
ϵ'_z = the internal axial strain in the pile.

Internal strains, stresses and forces in the piles are denoted by primed variables, and external stresses and forces are denoted by unprimed variables. Equation 1 is valid only if the confining soil stress-

es acting on the pile are small. A comparison of the measured magnitude of transverse strain to axial strain indicated that for the H-pile and the pipe pile the confining forces were small compared to the axial frost heaving forces (App. A).

The internal axial forces acting in the piles were calculated using the results from eq 1 and

$$F'_{z_i} = \sigma'_{z_i} A \qquad (2)$$

where F'_{z_i} = the internal axial force at depth i
σ'_{z_i} = the internal axial stress at depth i
A = the cross-sectional area of the pile (A = 94.2 cm² for the pipe pile and A = 155.0 cm² for the H-pile).

The frost-heave-induced shear stresses along the soil/pile interface were calculated from

$$\sigma_{xz} = (F'_{z_i} - F'_{z_j}) / (S_H \Delta z) \qquad (3a)$$

$$\sigma_{rz} = (F'_{z_i} - F'_{z_j}) / (S_P \Delta z) \qquad (3b)$$

where σ_{xz} = shear stress at the soil/pile interface from depth i to depth j for the H-pile
σ_{rz} = shear stress at the soil/pile interface from depth i to depth j for the pipe pile
F'_{z_i} = internal axial force acting at a depth greater than the internal axial force F'_{z_j} in the pile
S_H = surface area of the H-pile in m² per lineal meter
S_P = surface area of the pipe pile in m² per lineal meter
Δz = pile length in meters from depth i to depth j.

Average maximum shear stresses were calculated by dividing the peak uplift force by the surface area of the pile from the soil surface to the depth of the peak uplift force.

The strain, stresses and forces resulting from the ice collars and gravel layer could not be determined from the resistance strain gauge measurements since the field calibration results had determined that the upper strain gauges were not reliable (App. B). Consequently the effects of the ice and gravel layers on the piles had to be addressed indirectly.

Experiments on polycrystalline freshwater ice have shown that for long-term creep the deformation can be described by

$$\dot{\epsilon} = B(\tau_c)^n \qquad (4)$$

where $\dot{\epsilon}$ = strain rate in the ice
  B = constant that depends on the ice temperature, ice crystal fabric and other variations in ice properties
  τ_c = shear stress over the thickness of the ice collar at the ice/pile interface
  n = constant determined from experiments (Paterson 1981).

The magnitude of $\dot{\epsilon}$ can be estimated by using the measured rates of soil surface heave near the piles and the assumption that soil displacement is constrained only in a narrow region around the piles. Experimental results by Penner and Irwin (1969) and Saltykov (1944) indicate that soil surface heave is constrained only within 1 cm of a pile.

The strain rate in the ice was calculated from

$$\dot{\epsilon} = \tfrac{1}{2}(\Delta\dot{\mu}/\Delta y) \qquad (5)$$

where $\dot{\epsilon}$ = strain rate in the ice
  Δy = narrow region in which soil displacement is constrained (1 cm)
  $\Delta\dot{\mu} = \dot{\mu}_n - \dot{\mu}_0$
  $\dot{\mu}_n$ = soil surface displacement rate as measured near the pile
  $\dot{\mu}_0$ = soil surface displacement rate at the pile.

The soil surface displacement rate at the pile was assumed to be zero, a conservative assumption that will result in peak ice strain rates. The shear stress at the ice/pile interface over the thickness of the ice collar is found by combining eq 4 and 5 and solving for τ_c to obtain

$$\tau_c = (\dot{\epsilon}/B)^{1/n}. \qquad (6)$$

Table 2 gives values of B for $n = 3$ and several different temperatures from the experimental results reported by Paterson (1981). Representative values of B were determined for the ice temperatures measured in the study at or near the soil surface.

The uplift force on the piles at the ground surface due to an overlying ice collar was calculated from

$$F_c = \tau_c S_c t_c \qquad (7)$$

where F_c = uplift force on the pile at the ground surface due to an overlying ice collar

τ_c = shear stress at the ice/pile interface over the thickness of the ice collar
S_c = surface area of the pile in m² per lineal meter
t_c = thickness of the ice collar (m).

Shear stresses at the soil/pile interface from the ground surface to the depth of the first functioning strain gauge were determined from

$$\sigma_{xz_i} = (F'_{z_i} - F_c)/(S_H \Delta z) \qquad (8a)$$

$$\sigma_{rz_i} = (F'_{z_i} - F_c)/(S_P \Delta z) \qquad (8b)$$

where σ_{xz_i} = shear stress at the soil/pile interface for the H-pile from the ground surface to the depth of the first functioning strain gauge
  σ_{rz_i} = shear stress at the soil/pile interface for the pipe pile from the ground surface to the depth of the first functioning strain gauge
  F'_{z_i} = internal axial force on the pile at the depth of the first functioning strain gauge
  F_c = uplift force on the pile at the ground surface due to an overlying ice collar ($F_c = 0$) when there is no ice collar)
  Δz = pile length in meters from the ground surface to the depth of the first functioning strain gauge.

The depths to the first functioning strain gauge on the H-pile are nearly the same as the thickness of

Table 2. Values of flow law parameters (B) for different temperatures and n = 3 (from Paterson 1981).

T (°C)	B (s⁻¹ kPa⁻³)
0	5.3×10^{-15}
-5	1.7×10^{-15}
-10	5.2×10^{-16}
-15	3.1×10^{-16}
-20	1.8×10^{-16}
-25	1.0×10^{-16}
-30	5.4×10^{-17}
-35	2.9×10^{-17}
-40	1.5×10^{-17}
-45	7.7×10^{-18}
-50	3.8×10^{-18}

12

the gravel layer placed around the pile. Therefore, the heaving force on the H-pile due to the gravel layer for the last two winter seasons was calculated from

$$F_G = F_{z_i}' - F_c \qquad (9)$$

where F_G is the heaving force on the H-pile due to the gravel layer. The depths of the first functioning strain gauge on the pipe pile are greater than the thickness of the gravel layer. Consequently, the heaving force on the pipe pile due to the gravel layer was not determined.

Data acquisition periods

The H- and pipe piles were installed on 29 October 1982, and routine data acquisition began on 19 November after the installation of the instrument hut, electical power, and connection of all strain and temperature sensors to an HP 3497A datalogger. Soil surface heave had already begun and freezeback of the soil adjacent to the piles was complete by the time the datalogging was started. Strain and temperature measurements were automatically recorded at intervals varying between 2 and 12 hr throughout the study. Data acquisition for the 1982–83 season ended on 13 April 1983 before thaw consolidation occurred in the soil surrounding the piles. Data were obtained continuously (except for a few data gaps) for the 1983–84 and 1984–85 seasons, from 9 September 1983 to 6 May 1985. Unfortunately one of the data gaps (28 September to 20 October 1983) occurred at the beginning of the 1983–84 frost heave season, and so the onset of frost-heave-induced effects was missed. Consequently, the initiation of soil surface heave and the associated forces were not measured until the beginning of the 1984–85 season.

EXPERIMENTAL RESULTS

A common period of interest was selected for graphic presentation of the results of this study from 1 September 1982, 1983 or 1984 to 1 June 1983, 1984 or 1985. The frost heave season generally begins by mid-October and ends by late April or early May. This common period covers the initiation, occurrence and end of the frost heave season and allows direct comparison between the three winter seasons of data.

Air, ground, pile and ice collar temperatures

The air and ground temperatures for the 1982–83, 1983–84 and 1984–85 seasons are shown in Figures 14 and 15. There were five major low-temperature periods during each season when the air temperature dropped below –25°C for several days or more. Ground temperatures throughout the active layer above the permafrost measured at the thermistor string location in Figure 5 were at or below 0°C by early April for the first winter season and by early January for the last two winter seasons.

H- and pipe pile temperatures for the 1982–83, 1983–84 and 1984–85 seasons are shown in Figures 16 and 17. The soil around both piles was thawed to a depth of 0.5 m on 23–24 November 1982 by covering and heating the tops of the piles in an unsuccessful effort to establish an unstrained (thawed soil) reference for the strain gauges. The effect of this heating shows up as a temperature spike in the 1982–83 pile temperatures (Fig. 16 and 17). The temperatures along the H- and pipe piles were slightly lower than in the adjacent undisturbed ground. The pipe pile temperature was generally lower than the H-pile temperature during the winter, due to better thermal contact with the thermal siphon at depth.

Soil and pile temperatures were lower during the second and third winter seasons as a result of the roof structure sheltering the site (Fig. 15, 16 and 17).

The ice collars were formed by periodically pouring water into a 1.8-m-diam confining ring surrounding the tops of the piles and allowing it to freeze in layers. This resulted in the sudden temperature rises during the periods of 5 to 13 January 1983 and 16 to 20 November 1984 in Figures 16 and 17. Ice collars were not used on the piles during the 1983–84 winter season.

The ground surface surrounding the piles and thermistor string was lower during the last two years of the study due to thaw consolidation of the soil around the piles and the disturbances caused by placing the gravel layer and ice collars (Fig. 6). As a result, the upper temperature sensor on both piles and the thermistor string were no longer below ground. Consequently, the soil and pile temperature records for the last two seasons show the effect of the upper temperature sensor recording air or ice collar temperatures at or near the ground surface (Fig. 15, 16 and 17). The temperature data from the upper sensor on both piles were used to represent the ice temperature when computing the ice/pile shear stresses over the thickness of the ice collar.
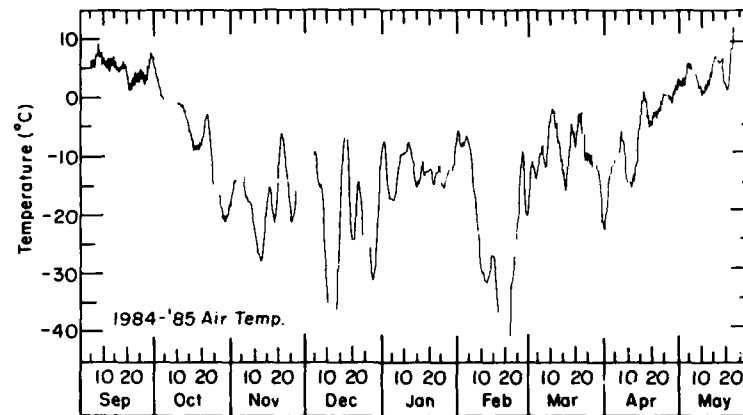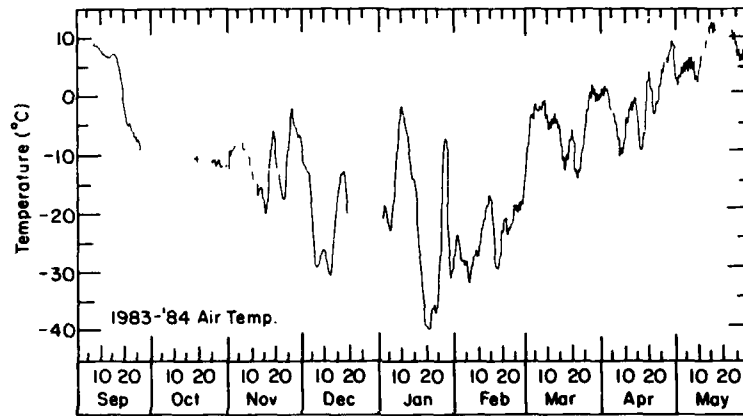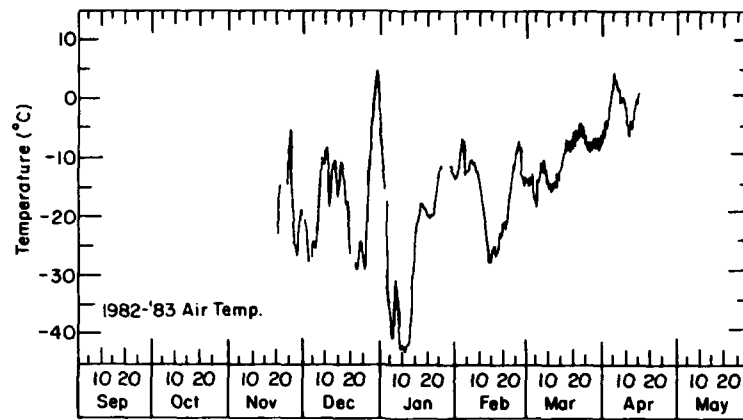
13

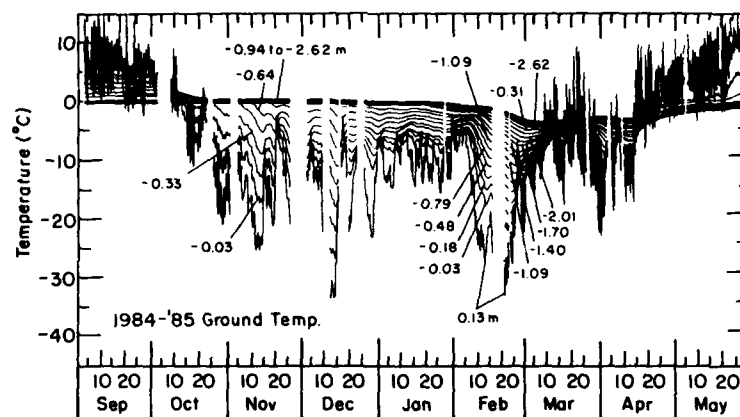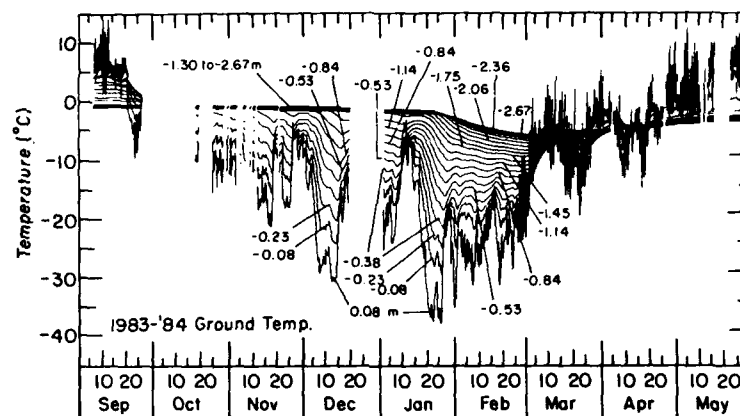*Figure 14. Air temperature for the 1982-83, 1983-84 and 1984-85 seasons.*
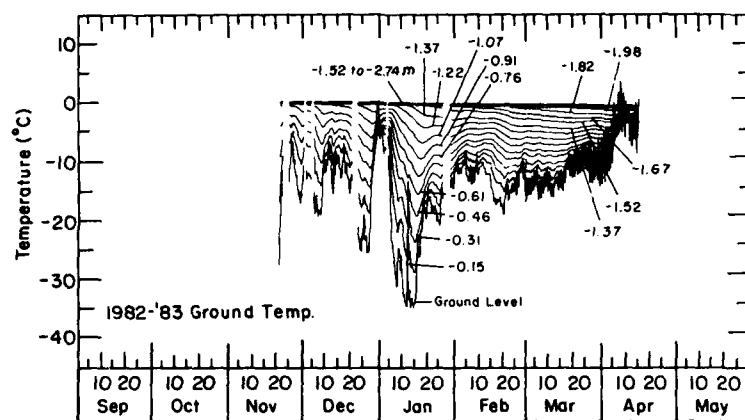
14

Figure 15. Ground temperature at different depths for the 1982-83, 1983-84 and 1984-85 seasons.

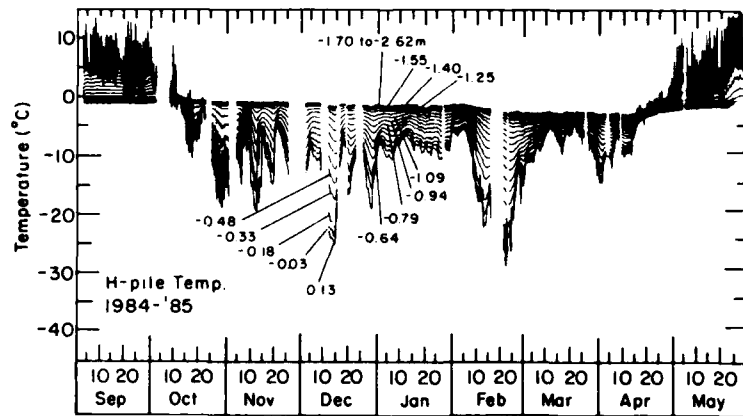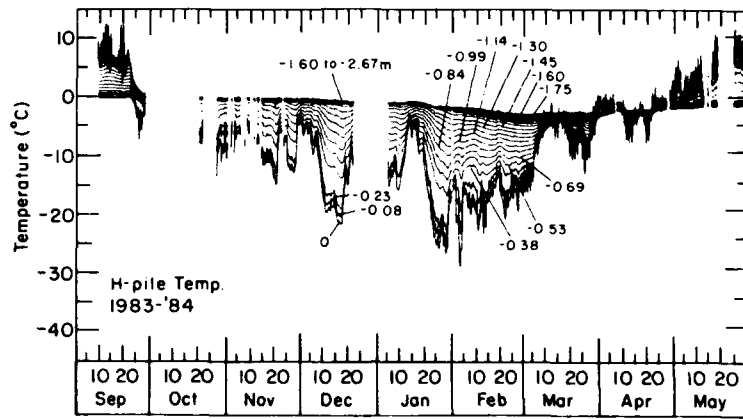*Figure 16. H-pile temperature at different depths for the 1982–83, 1983–84 and 1984–85 seasons.*
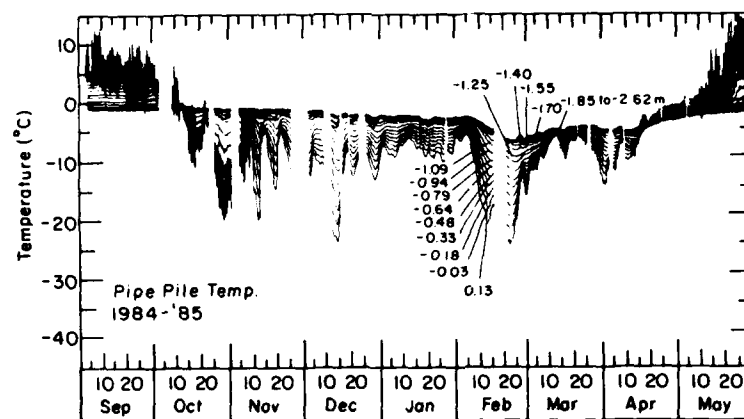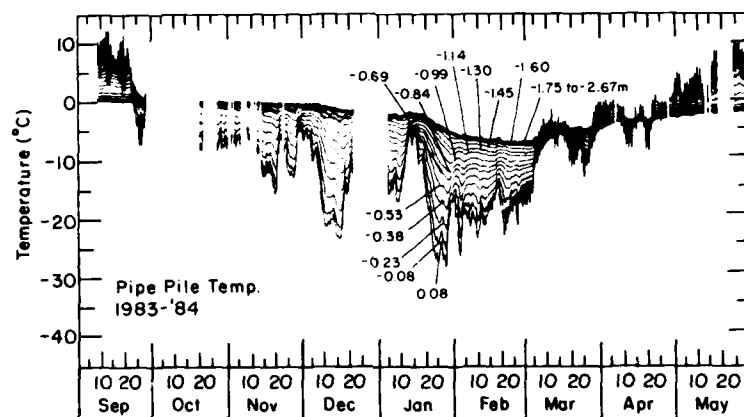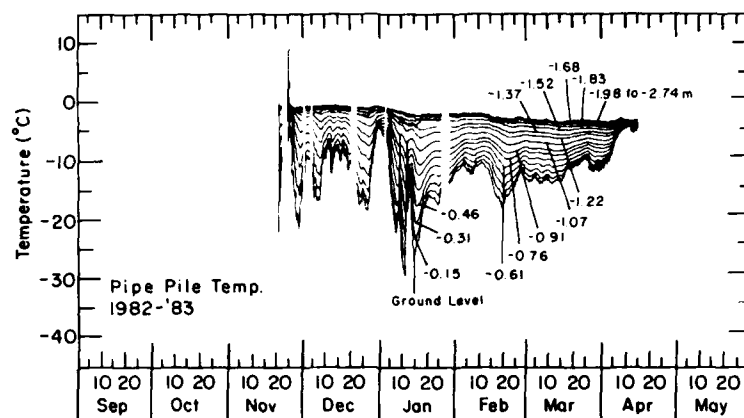
Figure 17. Pipe pile temperature at different depths for the 1982-83, 1983-84 and 1984-85 seasons.

17
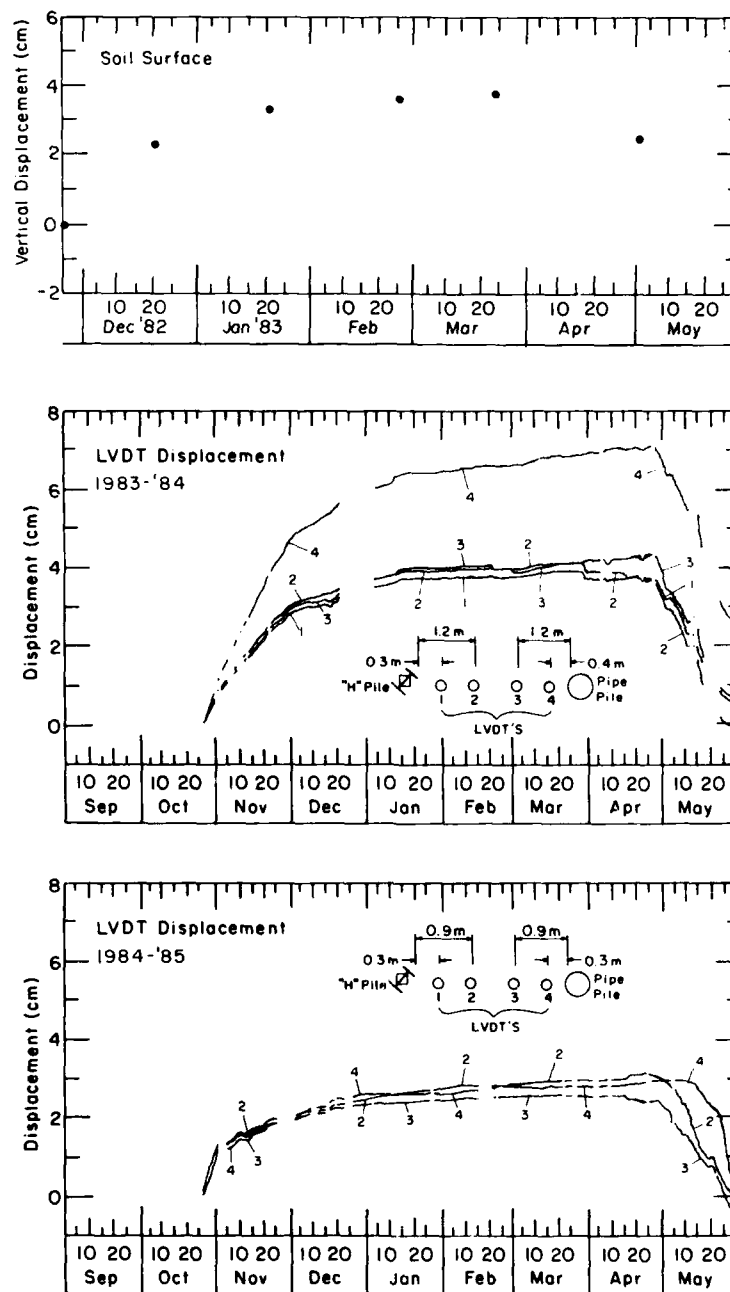
*Figure 18. Soil surface heave for the 1982-83, 1983-84 and 1984-85
seasons. LVDT displacements for points 1, 2, 3 and 4 indicate soil surface
displacements taken at the locations indicated.*

Pile stability and soil surface heave

The H-pile and the pipe pile did not heave during the first year of the study as shown in Figure 13, at least within the resolution of the survey methods (±1.0 mm). Subsequent surveys also showed that the piles were stable. The effectiveness of the thermal siphons and anchor rings/plates in refrigerating and anchoring the lower ends of the

test piles in the permafrost was demonstrated by the stability of the test piles. Figure 18 shows the soil surface heave for the 1982-83, 1983-84 and 1984-85 seasons. The ground surface displacements shown in Figure 18 may not represent the absolute or maximum accumulated displacements caused by frost heave since the measurements were not initiated at the onset of frost heave. Soil sur-

18

face displacements prior to the onset of frost heave were considered to be minimal. The large displacement of the soil indicated by the LVDT located 0.4 m from the pipe pile in 1983–84 relative to the displacements indicated by the other three LVDTs is probably the result of more frost heave in the vicinity of the pipe pile. Unfortunately, the LVDTs were reset during a data gap on 2 to 5 November 1984 (as shown by the obvious break in the 1984–85 soil displacements) and an ice collar was used around the piles, making it impossible to verify whether larger soil surface displacements again occurred in the vicinity of the pipe pile during the 1984–85 season. Soil surface displacements of 2 to 7 cm are indicated on Figure 18.

Forces and shear stresses

A true unconstrained reference used to determine strains was obtained for both piles during the field calibration tests on 20–21 June 1985, when the piles were completely freed of the surrounding soil by excavation and truly unloaded (App. B). These unstrained references were called common references since they were applied to all three seasons of data to determine the total strains, stresses, and forces on the piles. Figure 19 shows the total forces on the H-pile for all three seasons of the study. Both positive tensile (uplift) and negative compressive (resistive) forces are shown on the H-pile in Figure 19. The initial tensile load on the H-pile after installation is believed to be the loading on the pile caused by freezeback of the backfill slurry. The remnant compressive and tensile forces on the H-pile at the beginning and end of the 1983–84 and 1984–85 frost heave seasons are considered to be the result of the redistribution of forces resulting from consolidation of the adjacent soils (Fig. 19). The total forces shown in Figure 19 give the complete loading history, including the effects of soil thaw consolidation and frost-heave-induced uplift on the H-pile during the period of interest.

Three local references (one for each data season) were used to take in-situ strains into account and to determine frost heave strains, stresses and forces relative to the time of the local reference. The total forces relative to the common reference began to increase on the H-pile on 15 October 1984, the beginning of the 1984–85 frost heave season (Fig. 19). The first set of strain measurements taken on 15 October 1984 was selected as the local reference for the 1984–85 season. The selection of the local references for the 1982–83 and 1983–84 data sets was not as clear cut since the

onset of the total force increase was missed for both years (Fig. 19). The local references were selected as near as possible to the onset of the total force increase for the 1982–83 and 1983–84 seasons (24 November 1982 and 28 September 1983 respectively). Consequently, the frost heave force and shear stress values for the first two seasons do not represent the absolute or maximum values. The local references selected for the pipe pile were taken at the same times as those for the H-pile.

Frost heave forces for the three seasons covered in the study are shown in Figure 20 for the H-pile and Figure 21 for the pipe pile. Table 3 is a summary of the magnitude, times and depths of occurrence of the forces and shear stresses on both piles during the study.

Strains, stresses and forces could not be determined for the 1982–83 data set on the pipe pile since the field calibration results do not apply to the full bridge completion circuits used on the pipe pile during the 1982–83 season (App. B). During the study the pipe pile suffered the loss of 86% of the strain gauges on the pile. The few remaining good gauges appear to have given reliable results, which are given in Table 3 for the 1983–84 and 1984–85 seasons. The peak frost heave forces on the pipe pile were 43% higher and occurred earlier in the season and at a shallower depth than those for the H-pile. The magnitudes of frost heave forces and average soil/pile shear stresses for the pipe pile appear too high in comparison with the H-pile results and values reported by others. The pipe pile results should be considered suspect until verified by further research.

The peak forces on the H-pile were essentially the same for all three winter seasons, varying by only ±29 kN from the average peak force. The peak forces on the H-pile occurred late in the season and at an average depth of 2.2 m, which was 0.6 m below the top of the permafrost table during the last two winter seasons of the study (Table 3).

The calculated heaving force and ice/pile shear stress due to the ice collars are given in Table 3. The ice collars may have contributed 15 to 20% of the peak forces. These results were obtained using the indirect methods described in the "methods and materials" section, since all of the upper strain gauge sensors were unreliable (App. B). The ice/pile shear stresses given in Table 3 can vary considerably with changes in ice temperature and/or strain rate. Consequently, the calculated ice collar forces may be too high and should be used with caution. The average maximum soil/pile shear stresses given in Table 3 are computed on the
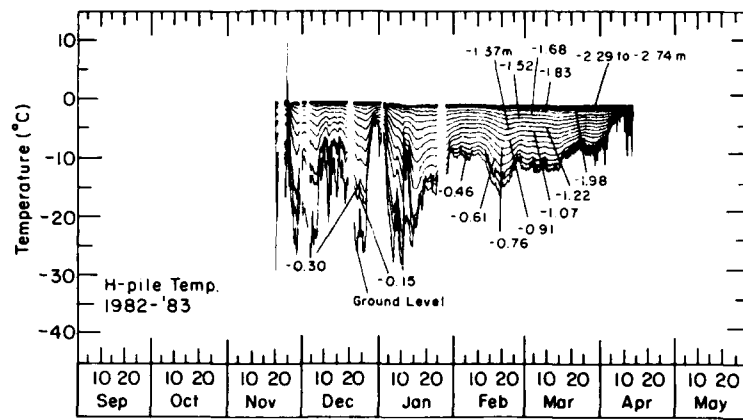
Figure 19. Total force on the H-pile at different depths for the 1982-83, 1983-84 and 1984-85 seasons.

20
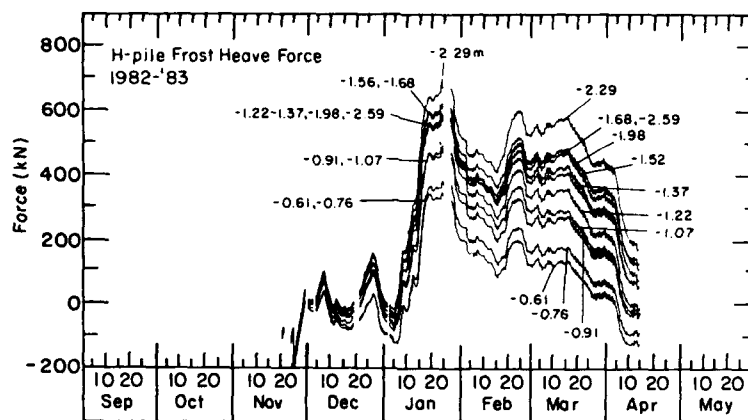
Figure 20. Frost heave force on the H-pile at different depths for the 1982-83, 1983-84 and 1984-85 seasons.

21

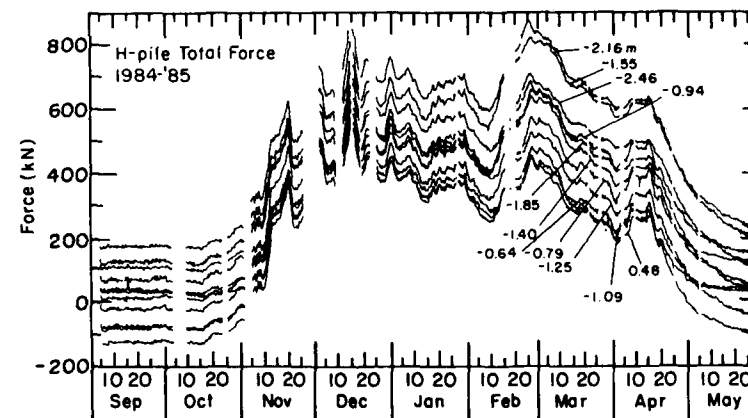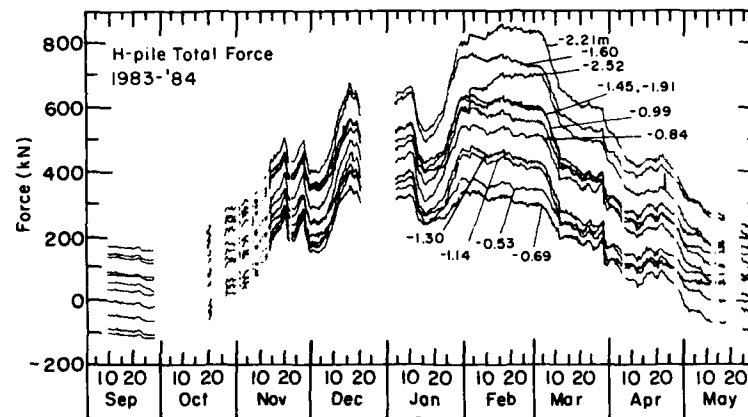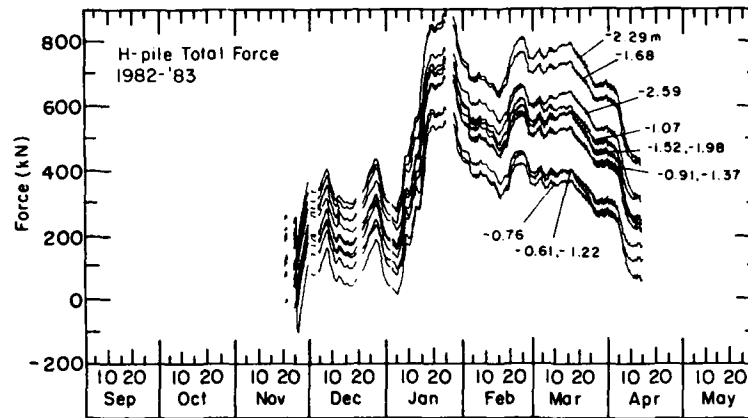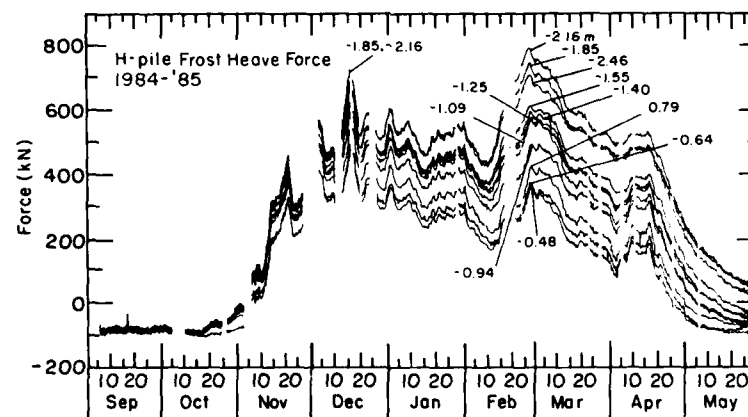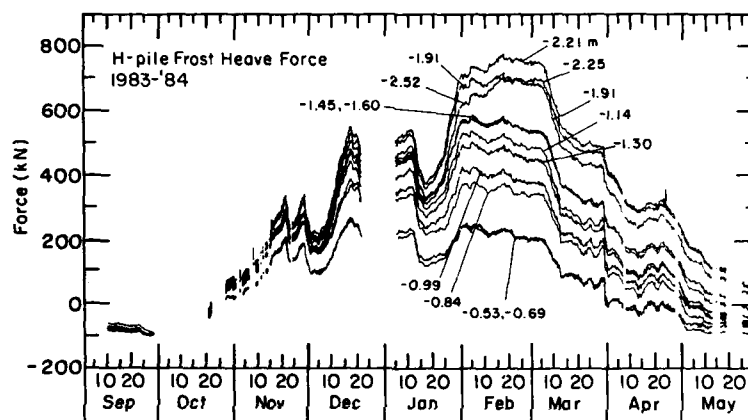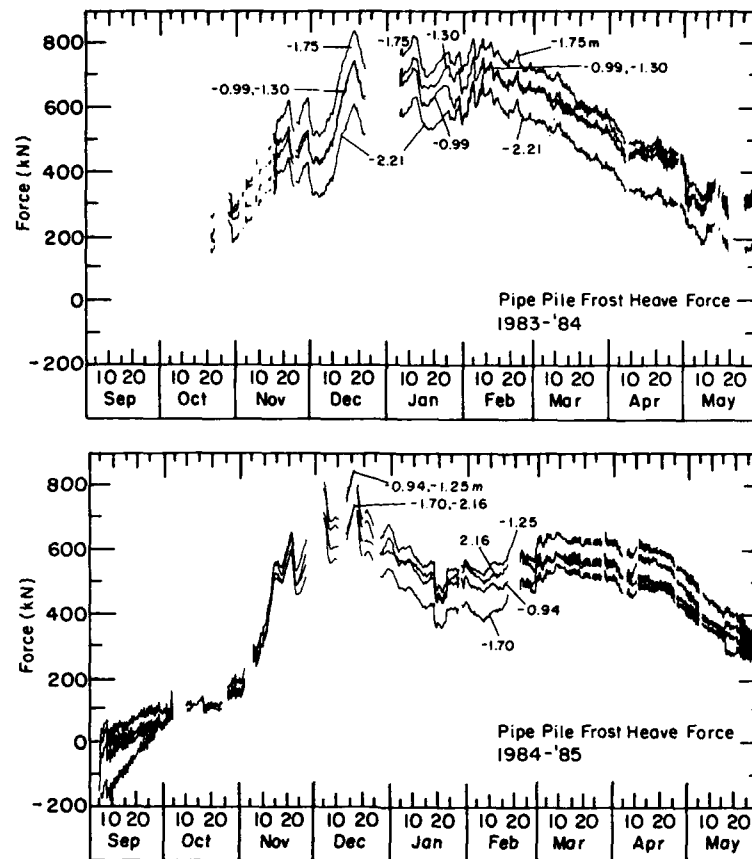*Figure 21. Frost heave force on the pipe pile at different depths for the 1983–84 and 1984–85 seasons.*

Table 3. Summary of maximum forces and average shear stresses on the H- and pipe piles.

	H-pile			*Pipe pile**	
	1982–83	*1983–84*	*1984–85*	*1983–84*	*1984–85*
Date peak frost heaving force occurred	24 Jan 83	17 Feb 84	26 Feb 85	17 Dec 83	15 Dec 84
Depth below ground surface where peak force occurred (m)	2.29	2.21	2.16	1.75	0.94
Peak frost heaving force (kN)	752	790	802	1118	1115
Thickness of the active layer between the piles at the beginning of the season (m)	2.3	1.6	1.6	1.6	1.6
Thickness of ice collar (m)	0.25	—	0.45	—	0.45
Heaving force due to ice collar (kN)[†]	151	—	118	—	185
Ice/pile shear stress due to ice collar (kPa)[†]	588	—	255	—	401
Maximum average soil/pile shear stress using the "boxed-in" ⊞ surface area of the H-pile (kPa)[**]	256	348	308	—	—
Maximum average soil/pile shear stress using actual surface area of the piles (kPa)[**]	157	214	190	627	972
Maximum internal stress in pile (MPa)	48.5	51.0	51.7	118.7	118.4
Heaving force due to gravel layer (kN)[†]	—	280	292	—	—

[*] The pipe pile results should be considered suspect until vertified by further research (see comments in text).

[†] The force and shear stresses for the ice and gravel layers had to be calculated indirectly (see text) and may be too high for the ice layer and consequently too low for the gravel layer.

[**] Computed using the pile surface areas from the soil surface to the depth of the peak frost heaving force on the pile.

22

basis of the "boxed in" (for the H-pile) and actual surface areas of the H- and pipe pile from the soil surface to the depth of the peak frost heave force on the piles. The 0.6-m-thick gravel backfill layer around the H-pile may have contributed about 35% of the peak forces measured on the pile during the second and third winter seasons (Table 3). The gravel backfill replaced the native soil around the tops of both piles. The higher peak forces measured on the pipe pile may be due to a larger contribution from the gravel layer; however, the force due to the gravel layer on the pipe pile could not be determined because of the lack of a reliable strain gauge on the upper portion of the pile.

Figures 22 and 23 show the pile temperature, shear stress distribution and frost heave force on the H-pile during the 1984–85 season on the 15th of each month from October through May. The shaded area shows the shear stress distribution between the levels at which strain gauges were functioning properly for the H-pile. The ice/pile shear stress and the uplift force due to the ice collar are shown above the ground surface or zero depth value. Soil/pile shear stresses are not uniform along the length of the pile, but vary considerably in sign and magnitude over time and depth. Generally the uplift shear stresses due to frost heaving act from the ground surface to the depth of the maximum force on the pile, and the restraining shear stresses act from the depth of the maximum force on the pile downward until the uplift force is balanced. However, there are zones of resistive soil/pile shear stresses which reduce the frost heave force on the pile between the soil surface and the depth of the peak force. These resistive soil/pile shear stresses and the corresponding reduction in frost heave force are larger than values that could be attributed to the variability associated with the estimate of Young's modulus for the gauges. The zones of resistive soil/pile shear stress may be due to bands of slightly different soil type or moisture/ice content. A detailed investigation of soil type and moisture/ice content with depth and time is needed to adequately investigate the zones of resistive shear stress between the soil surface and the depth of the peak force. The top of the permafrost table was at a depth of 1.6 m at the beginning of the 1984–85 winter season. The depth of the maximum force on the H-pile was 0.6 m below the top of the permafrost table during the 1984–85 season. Uplift soil/pile shear stresses are present in the permafrost throughout the winter.

The majority of experiments to measure frost heaving forces acting on piles have been conducted on piles embedded in non-permafrost soil. In analyzing the results of those experiments it has been implicitly assumed that once the soil temperature is lower than 0°C (i.e. when the soil is frozen) that soil heave and frost heaving forces are negligible. The results of our experiments and those of Crory and Reed (1965) indicate that soil heave and frost heave forces continue to be generated throughout the winter even in frozen ground (Fig. 18, 19 and 20). Ground temperatures throughout the active layer above the permafrost were at or below 0°C by early April for the first winter season and by early January for the last two winter seasons (Fig. 15). Peak frost heave forces occurred on the piles when the soil temperatures were below 0°C at depths below the top of the permafrost table. Significant soil heaving occurred after all ground temperatures fell below 0°C (Fig. 18). A comparison of Figures 18–20 shows that the soil heave rate is very small during the period of maximum uplift forces.

That soil heave and increases in pile uplift forces are occurring even when soil temperatures are below 0°C leads us to hypothesize an explanation that incorporates the existence and migration of unfrozen water within the frozen soil. Experiments have shown that a mixture of ice and unfrozen water is present in soils at temperatures below 0°C. Experiments have also shown that a frozen soil containing both ice and unfrozen water that is subjected to a temperature gradient causes water to move toward the colder soil (Dirkson and Miller 1966, Oliphant et al. 1983). The resulting migration of water toward the colder soil tends to enhance ice lens formation and consequently soil heaving. The water migration continues until the unfrozen water and ice content in the source zone is reduced to insignificant levels (Tice et al. 1982). Measurements of unfrozen water content as a function of temperature for soils show that the percentage of unfrozen water decreases exponentially with decreasing temperature (Fig. 24). Experiments on Fairbanks silt indicate that frost heaving may be insignificant for soil temperatures in Fairbanks silt below -2°C (Anderson and Morgenstern 1973).

The unfrozen water content–temperature relationship may explain why the heave forces acting on piles embedded in permafrost respond so rapidly to temperature changes. On cooling, the unfrozen water will migrate toward the colder soil, causing an increase in ice lens growth, and the percentage of unfrozen water will decrease exponentially as a function of temperature. This may con-

Figure 22. Pile temperature, shear stress distribution (shaded area), and force as a function of depth for the H-pile during the 1984–85 season. a—15 October 1984; b—15 November 1984; c—15 December 1984; d—15 January 1985.
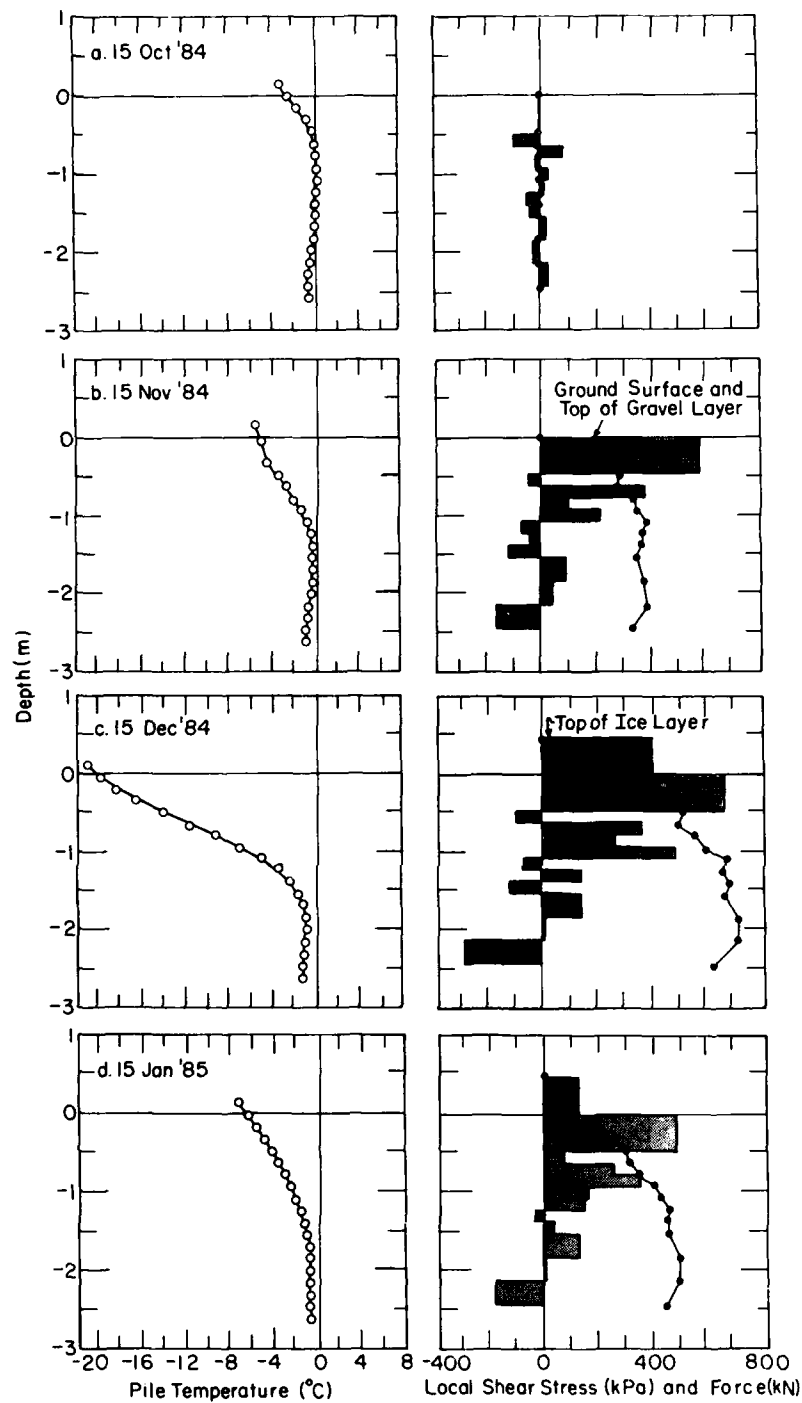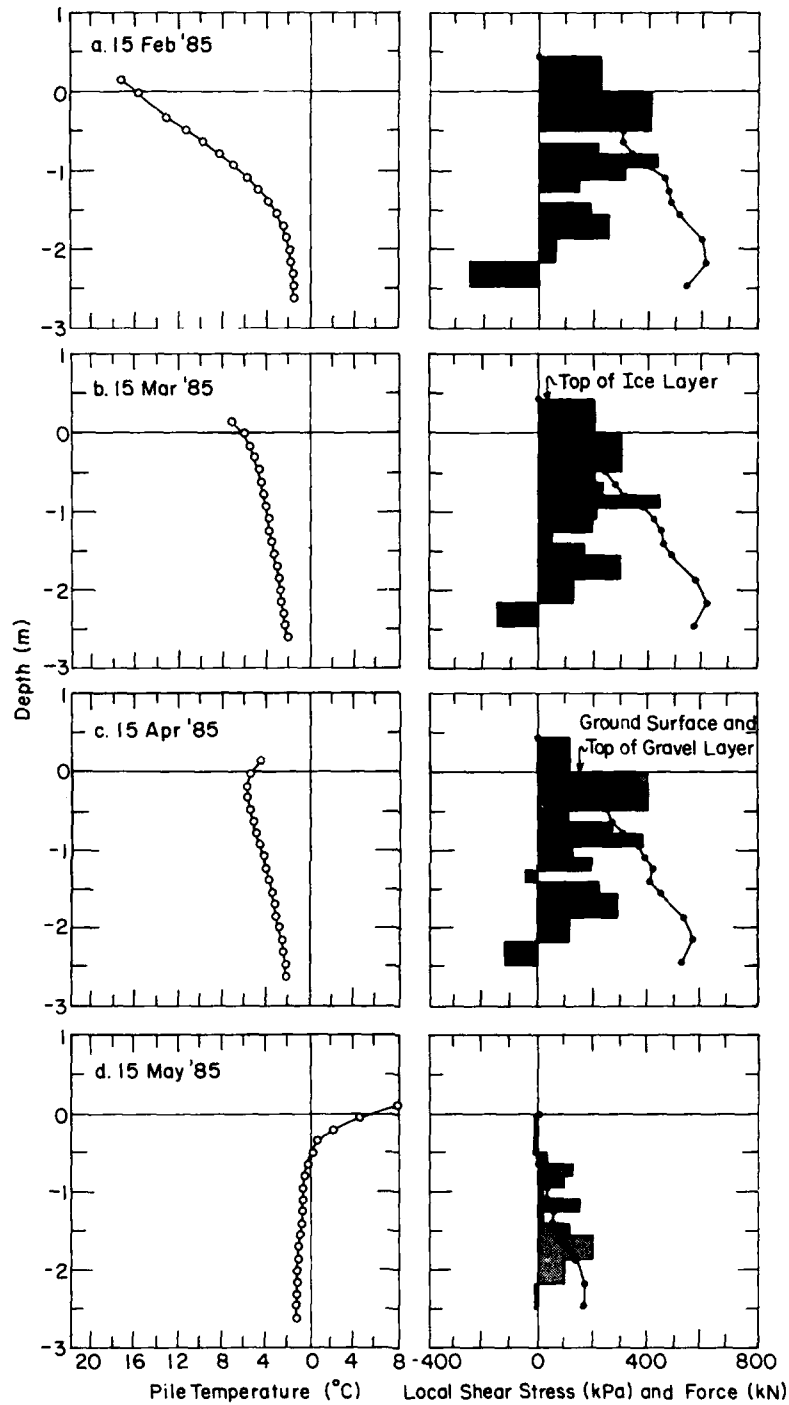
24

Figure 23. Pile temperature, shear stress distribution (shaded area), and force as a function of depth for the H-pile during the 1984–85 season. a—15 February 1985; b—15 March 1985; c—15 April 1985; d—15 May 1985.
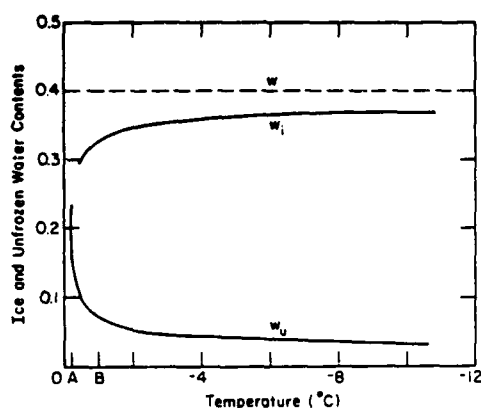
25

Figure 24. Unfrozen water and ice contents in Fairbanks silt (after Fish 1985). Rate of maximum freezing occurs at A for unfrozen soil and at B for soils that are cooling and the highest temperature is − 1 °C.

tribute to increased heave forces. On warming, the percentage of unfrozen water will increase exponentially as a function of temperature, resulting in a decrease in heave forces. The rapid change in unfrozen water content will also result in a significant change in the mechanical properties of the soil. An increase in unfrozen water content will reduce soil shear strength, resulting in increased creep and lower shear stresses and forces on the piles.

The ice and unfrozen water content vs temperature relationship for in-situ soils may be useful in developing a method for designing pile installations in both permafrost and unfrozen soils. During soil cooling, soil temperature measurements and the relationship between the percentage of unfrozen water and temperature for the soil could be used to determine the depth of maximum freezing rate (i.e. the depth at which unfrozen water is being most rapidly converted to ice) in the soil, which ultimately is related to the depth over which shear stresses and uplift forces act on a pile. This depth may possibly be determined from the slope of the ice and unfrozen water conent vs temperature curve (Fig. 24). The depth of maximum heave force might be expected to coincide with the depth of most rapid freezing. This depth depends on the soil temperature and will vary with soil type. For non-permafrost soils the depth of most rapid freezing is near the 0°C isotherm (it usually occurs at temperatures somewhat lower than 0°C; Fig. 24). For permafrost soils the depth to the maximum rate of freezing may still be useful in establishing pile installation designs. This can be ac-

complished by monitoring the soil temperature as a function of depth and time throughout a winter. The soil temperatures are used with the ice and unfrozen water content curves to estimate the depths of maximum freezing rate over time. The depth of maximum freezing rate is then used when calculating the depth of action for frost heaving stresses over time. Currently few ice and unfrozen water content vs temperature relationships have been determined, and their dependence on initial soil water content have been poorly investigated. A large number of ice and unfrozen water content relationships for different soils would have to be determined before the proposed pile installation design method could be routinely used.

Spatial and temporal location of peak forces

Figures 25, 26 and 27 give comparisons of air temperature, ground temperature as a function of depth and time, and H-pile frost heave force and temperature as functions of depth and time for the 1982-83, 1983-84 and 1984-85 seasons, respectively. Figures 28 and 29 give similar comparisons for the 1983- and 1984-85 seaons for the pipe pile. The spatial and temporal location of the maximum force on the piles for each season is indicated on Figures 25-29. The highest uplift forces acting on the piles occurred during the coldest periods of the winter (Fig. 25-29). The forces for both piles generally increased after a decrease in air temperature and decreased after an increase in air temperature. Changes in the forces acting on the piles usually lagged behind corresponding air temperatures from 1 to 8 days, with the longer lag times occurring later in the winter season. This was caused by the time required for an air temperature wave to propagate into the soil. Soil temperature changes at depth may affect the forces acting on the piles by changing the rate of soil heaving, the amount of unfrozen water in the soil, the adfreeze strength of the soil adjacent to the piles, or the creep properties of the soil, or by causing differential thermal expansion between the piles and the soil. The maximum forces (Fig. 25-29) do not necessarily coincide with the 0°C isotherm as has been assumed in past studies. During the last two years of the study the peak frost heave forces on the H-pile occurred at an average depth of 2.2 m, which is within the permafrost zone (Fig. 25-27). The shallower average depth of 1.4 m for the peak uplift forces on the pipe pile (Fig. 28 and 29) may be the result of the pipe pile/soil interface being colder due to better thermal contact with the thermal siphon at depth. In the spring, uplift forces

26

Figure 25. Comparison of air temperature, ground temperature as a function of depth and time, and H-pile frost heave force and temperature as a function of depth and time for the 1982–83 season.

27

Figure 26. Comparison of air temperature, ground temperature as a function of depth and time, and H-pile frost heave force and temperature as a function of depth and time for the 1983–84 season.

28

Figure 27. Comparison of air temperature, ground temperature as a function of depth and time, and H-pile frost heave force and temperature as a function of depth and time for the 1984–85 season.

29

Figure 28. Comparison of air temperature, ground temperature as a function of depth and time, and pipe pile frost heave force and temperature as a function of depth and time for the 1983–84 season.
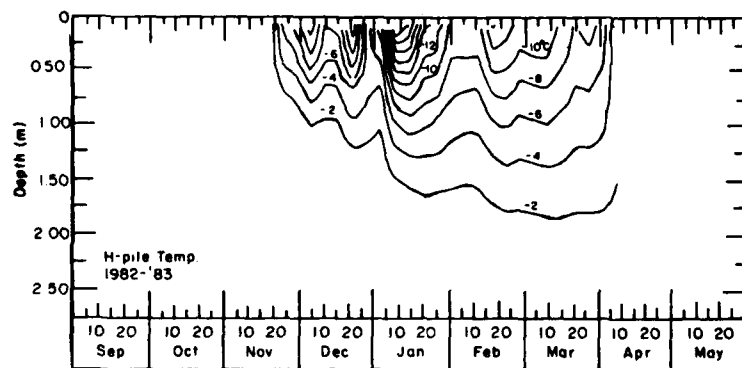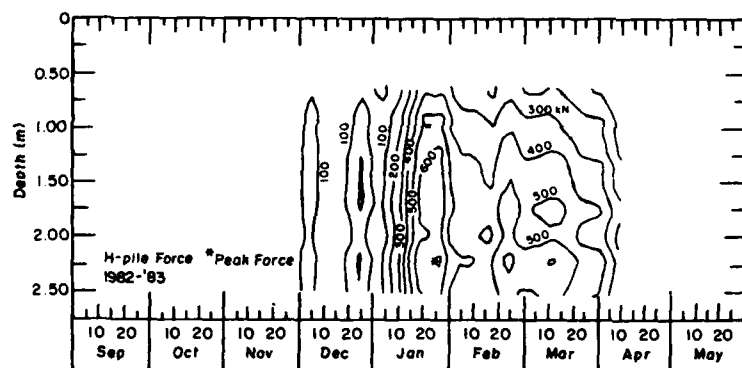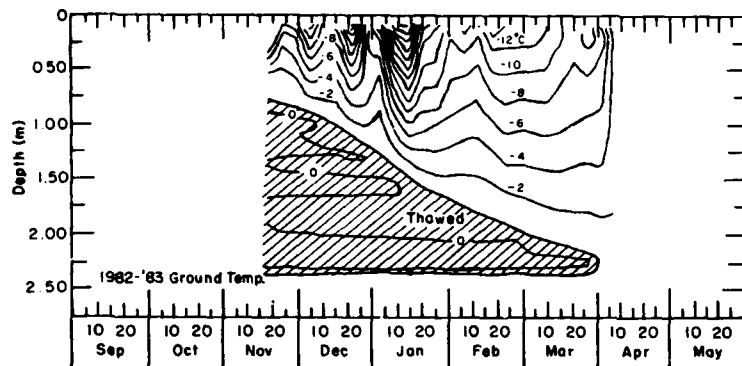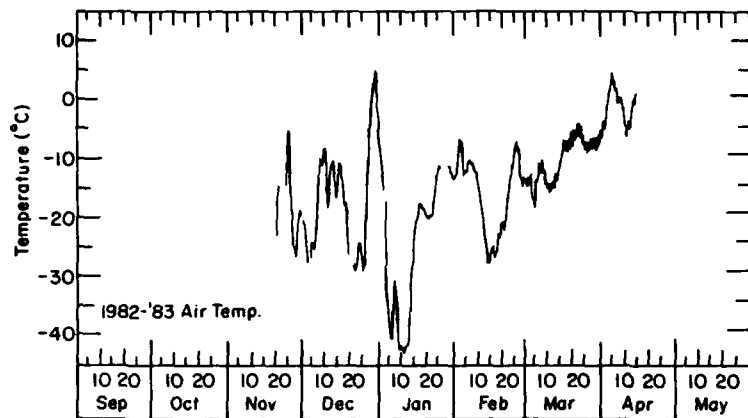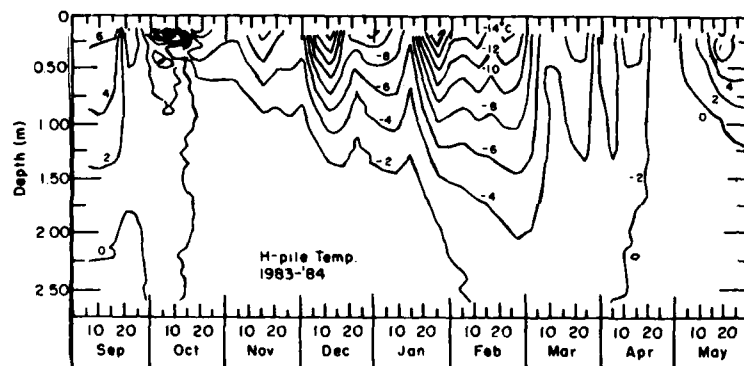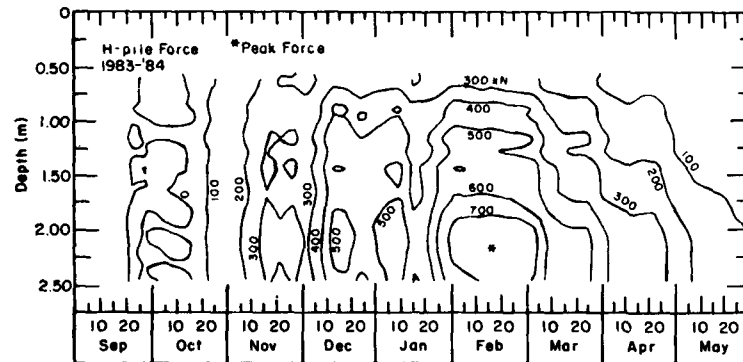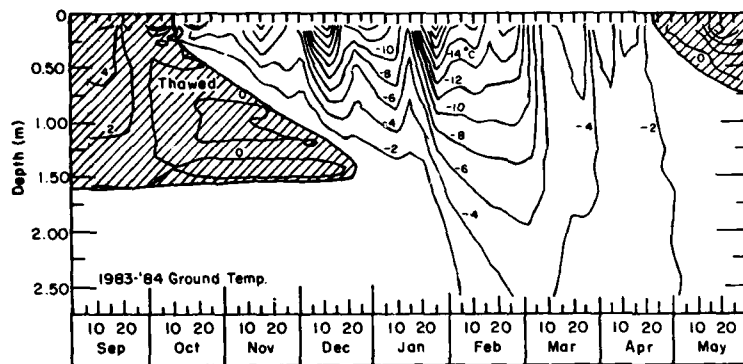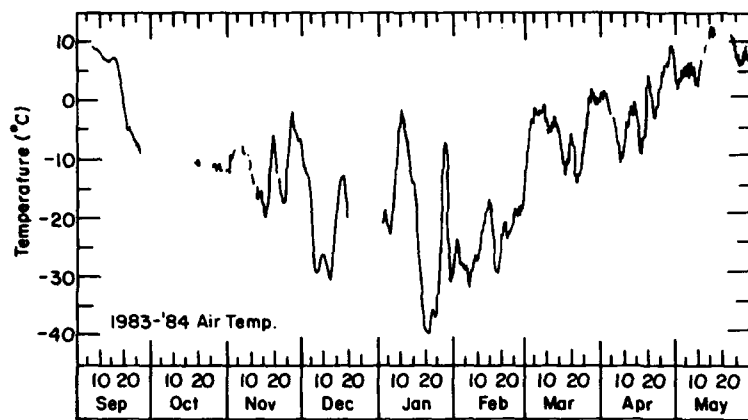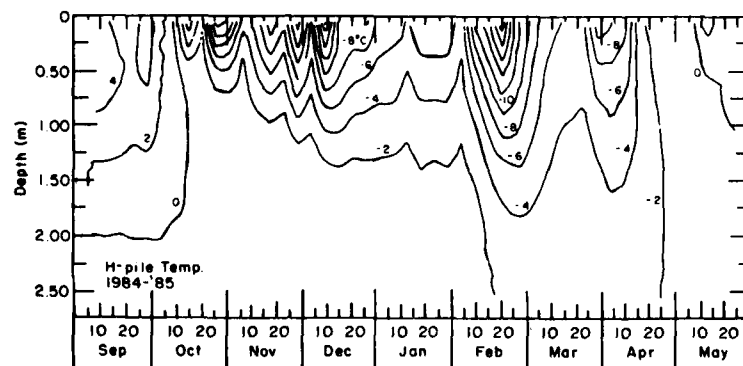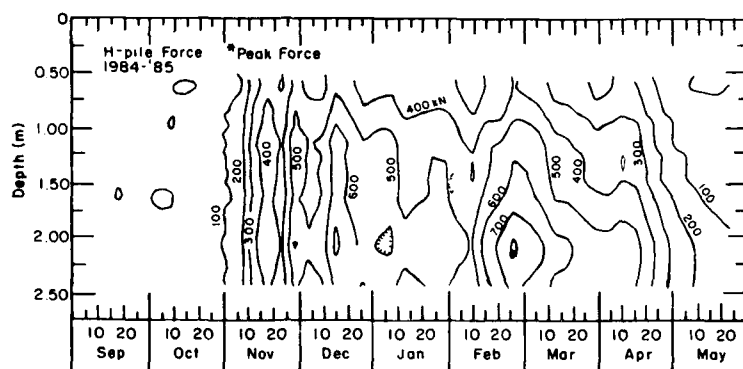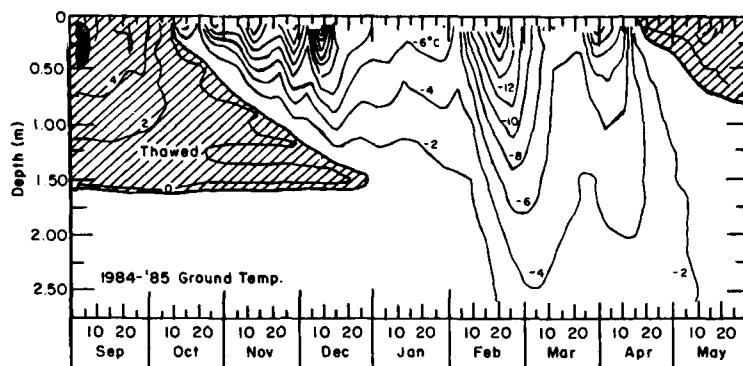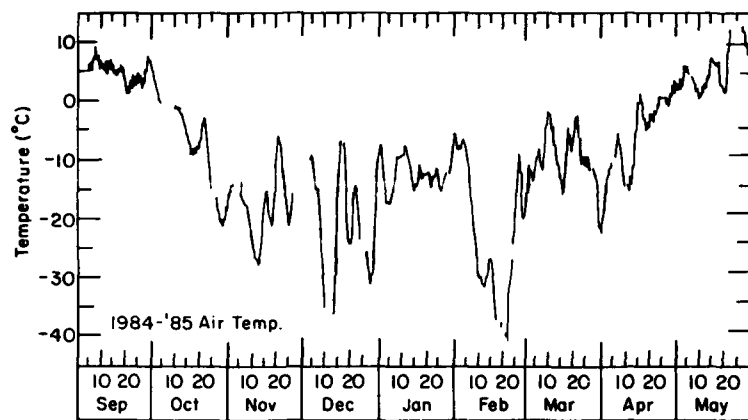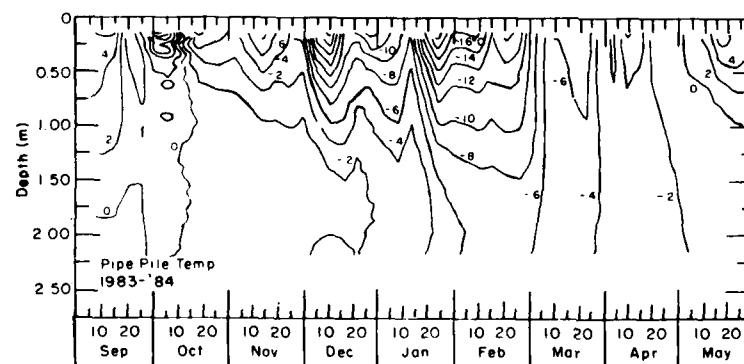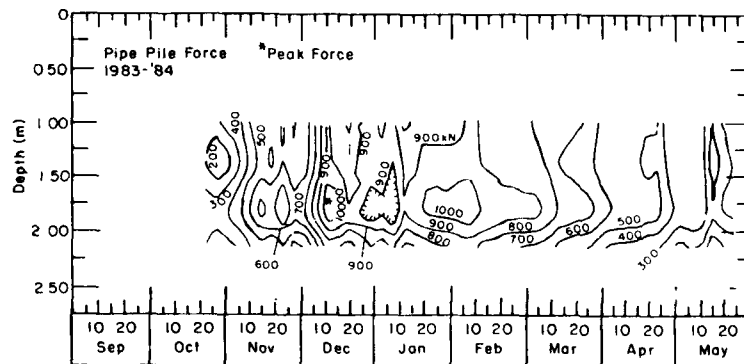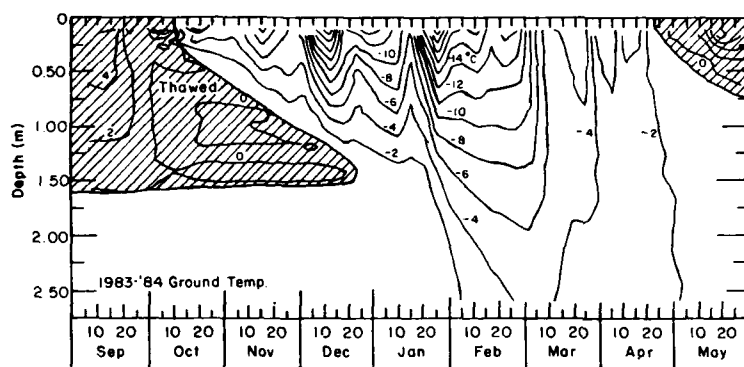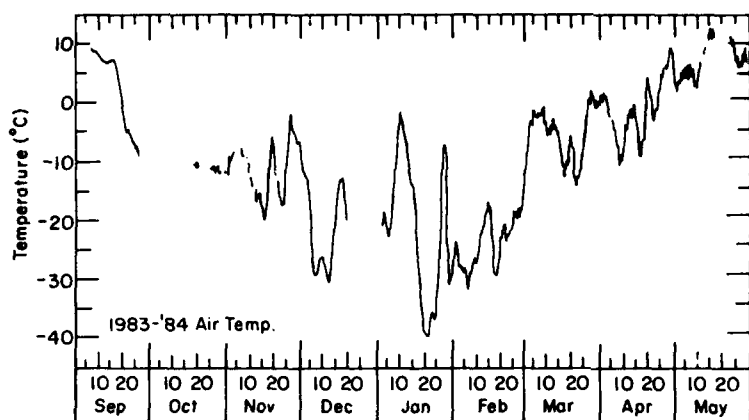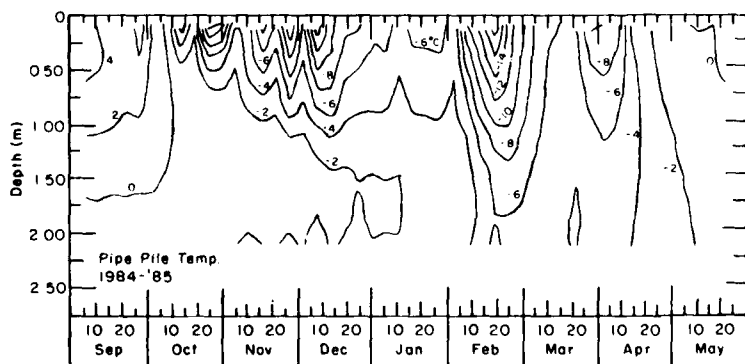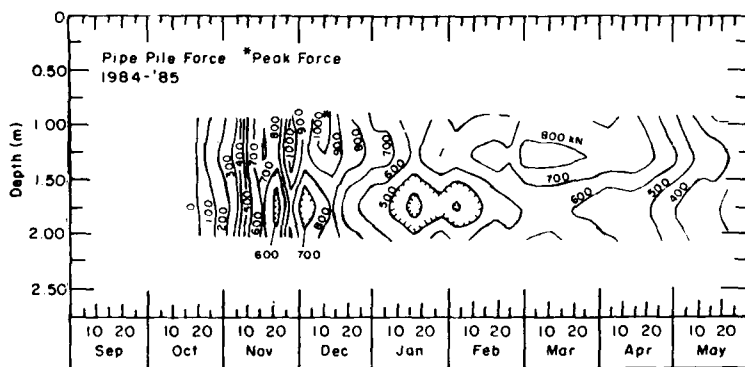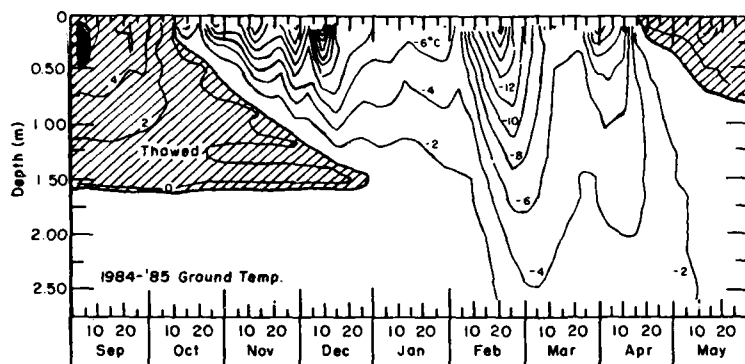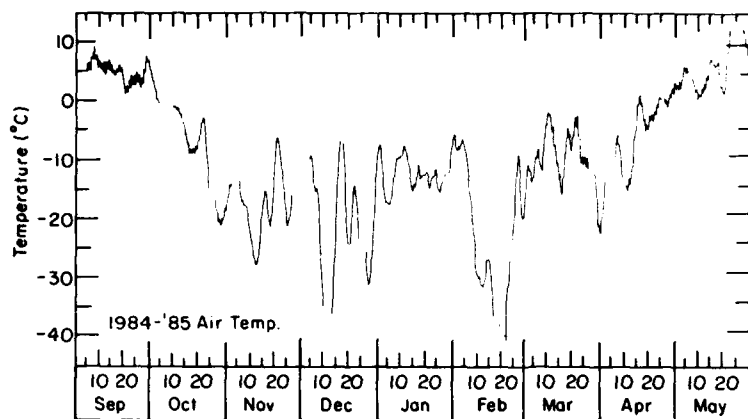
30

Figure 29. Comparison of air temperature, ground temperature as a function of depth and time, and pipe pile frost heave force and temperature as a function of depth and time for the 1984–85 season.

31

are relieved from the surface down as the ground warms. A general reduction in force values also occurs over the full length of the piles (Fig. 25-29).

CONCLUSIONS

Calculated forces, as determined from the instrumented piles, indicate that the magnitude of frost-heaving uplift forces acting on a pile increases from the soil surface to a maximum value at depth, then decreases due to the restraining action of the soil or permafrost on the pile (Fig. 22 and 23). The depth of maximum forces does not necessarily coincide with the 0°C isotherm, as has been assumed in past studies. Therefore, average soil/pile shear stresses should be calculated on the basis of the pile surface area from the soil surface to the depth of the peak frost heave force when calculating shear stress from measured uplift forces. The average depths of the maximum frost heave forces were 2.2 m on the H-pile and 1.4 m on the pipe pile. The peak frost heave forces on the H-pile during the three winters of study were 752, 790 and 802 kN. The peak frost heave forces on the pipe pile during the second and third winter seasons of the study were 1118 and 1115 kN. Maximum internal tensile stresses on the H-pile were 48.5, 51.0 and 51.7 MPa during the three winters. Maximum internal tensile stresses on the pipe pile were 118.7 and 118.4 MPa for the second and third winter seasons. The heave forces that may have been contributed by the ice collars at the top of the piles during the 1982-83 and 1984-85 seasons were 151 and 118 kN, respectively, for the H-pile and 185 kN during the third winter season on the pipe pile. The heave forces that may have been contributed by the gravel layer around the top of the H-pile during the 1983-84 and 1984-85 seasons were about 280 and 292 kN, respectively.

Maximum average soil/pile shear stresses computed on the basis of the "boxed in" surface area of the H-pile from the soil surface to the depth of peak frost heave force were 256, 348 and 308 kPa during the three winters. Maximum average soil/pile shear stresses computed using the actual surface areas of the piles from the soil surface to the depth of the peak frost heave force were 157, 214 and 190 kPa during the three winters on the H-pile, and 627 and 972 kPa during the second and third winter seasons on the pipe pile. Calculated ice/pile shear stresses due to the ice collars at the tops of the piles were 588 and 255 kPa for the H-pile and 401 kPa for the pipe pile during the winters that ice collars were in place.

The forces and stresses resulting from the ice and gravel layers could not be determined directly due to strain gauge malfunctions. The forces and stresses were calculated indirectly and may be too high for the ice layer and consequently too low for the gravel layer.

Maximum heaving forces and shear stresses occurred during periods of maximum cold and soil surface heave. These forces were not related to the depth of frost for most of the winter since the soil adjacent to the piles was frozen to the permafrost table. The forces for both piles generally increased after a decrease in air temperature and decreased after an increase in air temperature. Changes in forces acting on the piles usually lagged behind corresponding air temperature changes by several days.

The highest rates of soil surface heave occurred from the onset of heave in October to the end of December, and then the heave rates decreased through the rest of the winter. Soil surface displacements of 2 to 7 cm were measured at the experiment site.

The important mechanisms that determine the magnitude of uplift heave forces are 1) soil heaving as the driving force, and 2) soil temperature, which controls the unfrozen water content, the mechanical properties of the soil and the area of influence of heaving pressures.

The higher forces and shear stresses on the pipe pile in this study may be the result of the soil/pile interface being colder than that of the H-pile because of better thermal contact with the thermal siphon at depth. The pipe pile results are considered suspect until verified by further research.

It is beyond the scope of this study to develop a method for designing pile installations in permafrost. However, an outline of how the results of this study might be used to design pile installations is presented below.

Past design methods for pile installations in soil subjected to frost heaving have utilized the 0°C isotherm as the reference to determine average expected shear stresses and uplift forces. This method may not be useful when permafrost is present and a unique 0°C isotherm does not exist. We suggest an alternative method of designing pile installations using the unfrozen water content-temperature relationship for the in-situ soil type. During soil cooling, soil temperature measurements and the percent unfrozen water-temperature relationship for the soil could be used to determine the depth of maximum freezing rate (i.e. the depth at which unfrozen water is being most rapidly converted to ice) in soil, which ultimately is related to

the depth over which shear stresses and uplift forces act on a pile. This depth can be determined from the slope of the ice and unfrozen water content vs temperature curve (Fig. 24). The depth of maximum heave force might be expected to coincide with the depth of most rapid freezing. This depth depends on the soil temperature and will vary with soil type. For non-permafrost soils the depth of most rapid freezing is near the 0°C isotherm (it usually occurs at temperatures somewhat lower than 0°C; Fig. 24). For permafrost soils the depth to the maximum rate of freezing may still be useful in establishing pile installation designs. This can be accomplished by monitoring soil temperature as a function of depth and time throughout a winter. The soil temperatures are used with the ice and unfrozen water content curves to estimate the depths of maximum freezing rate over time. The depth of maximum freezing rate is then used when calculating the depth of action for frost heaving stresses.

RECOMMENDATIONS

The following recommendations are offered at the conclusion of this study:

1. The use of electric strain gauges as a method of measuring and determining frost heave forces on piles is recommended, since they take uplift and resistive shear stresses into account to determine the magnitude of peak forces on a pile and provide information concerning the spatial and temporal location of the forces. Soil/pile shear stress distributions along the pile can be determined from the results provided by this method. Quarter bridge gauge configurations and redundant strain gauges are recommended to provide better reliability, allow for easier data interpretation and accommodate the relatively high failure rate of strain gauges. Gauge calibration is required at the beginning and end of the experiment to verify the applicability of the initial calibration.

2. Further evaluation should be made of the H-pile data set, as this may lead to a method of estimating the depth and timing of the peak force that would take into account the effect of unfrozen water on the frost heave forces.

3. Continued research on the unfrozen water–temperature relationship for frost-susceptible soils is recommended, as it may contribute to a better method of designing pile installations in permafrost and non-permafrost regions. Present design methods for pile installations in soils subjected to frost heaving utilize the 0°C isotherm as the reference to determine expected shear stresses and uplift forces. This method may not be useful in permafrost where a unique 0°C isotherm does not exist.

4. The pipe pile results need verification and the effects of the thermal siphon should be studied further. A comparative approach is recommended that uses a pipe pile without a thermal siphon and one with a thermal siphon. The adfreeze effects of an ice layer and gravel backfill should also be investigated using a similar comparative approach.

5. The influence of ice collars and different fill materials should be further investigated. Strain gauge malfunctions during this study prevented us from determining the force contribution resulting from the ice and gravel layers in a direct manner.

LITERATURE CITED

Anderson, D.M. and N.R. Morgenstern (1973) Physics, chemistry and mechanics of frozen ground. In *Permafrost: North American Contribution to the Second International Conference, 13–28 July, Yakutsk, U.S.S.R.* Washington, D.C.: National Academy of Sciences, p. 257–288.

Crory, F.E. and R.E. Reed (1965) Measurement of frost heaving forces on piles. USA Cold Regions Research and Engineering Laboratory, Technical Report 145. AD 484 955.

Dirksen, C. and P.J. Miller (1966) Closed-system freezing of unsaturated soils. *Soil Science Society of America Proceedings,* 30: 168–173.

Domaschuk, L. (1982) Frost heave forces on embedded structural units. In *Proceedings, Fourth Canadian Permafrost Conference,* p. 487–496.

Esch, D.C. (1982) Thawing of permafrost by passive solar means. In *Proceedings, Fourth Canadian Permafrost Conference,* p. 560–569.

Esch, D.C. (1983) Permafrost prethawing by surface modification. Alaska Department of Transportation Report AK-RD-83-23.

Fish, A.M. (1985) Creep strength, strain rate, temperature and unfrozen water relationship in frozen soil. In *Proceedings, Fourth International Symposium on Ground Freezing, Sapporo, Japan,* vol. 2, p. 29–36.

Johnson, J.B. and D.C. Esch (1985) Frostjacking forces on H- and pipe piles embedded in Fairbanks silt. In *Proceedings, Fourth International Symposium on Ground Freezing, Sapporo, Japan,* vol. 2, p. 125–133.

Johnston, G.H. and B. Ladanyi (1972) Field studies of grouted rod anchors in permafrost. *Canadian Geotechnical Journal,* 9(2): 176–194.

Kinosita, S. (1967) Heaving force of frozen soils. In *Proceedings, International Conference on Low Temperature Science*, vol. 11, p. 1345–1360.

Kinosita, S. and T. Ono (1963) Heaving forces of frozen ground. Mainly on the results of field research. Low Temperature Science Laboratory Teron Kagaku, Ser. A-21, p. 117–139. (National Research Council Technical Translation 1246, 1966.)

Kinosita, S., Y. Suzuki, K. Horiguchi and M. Fukuda (1978) Observations of frost heaving action in the experimental site, Tomakamai, Japan. In *Proceedings of the Third International Conference on Permafrost, July 10–13, 1978, Edmonton, Alberta, Canada*, vol. 1, p. 676–678.

Linell, K.A. (1973) Long-term effects of vegetation cover on permafrost stability in an area of discontinuous permafrost. In *Permafrost: North American Contribution to the Second International Conference, 13–28 July, Yakutsk, U.S.S.R.* Washington, D.C.: National Academy of Sciences, p. 688–693.

Oliphant, J.L., A.R. Tice and Y. Nakano (1983) Water migration due to a temperature gradient in frozen soil. In *Proceedings, 4th International Conference on Permafrost, 17–22 July, Fairbanks, Alaska*. Washington, D.C.: National Academy Press, p. 951–956.

Paterson, W.S.B. (1981) *The Physics of Glaciers*. New York: Pergamon Press, p. 20–41.

Penner, E. (1970) Frost heaving forces in Leda clay. *Canadian Geotechnical Journal*, 7(1): 8–16.

Penner, E. (1972) Influence of freezing rate on frost heaving. *Highway Research Board Record*, No. 393: 56–64.

Penner, E. (1974) Uplift forces on foundations in frost heaving soils. *Canadian Geotechnical Journal*, 11(3): 323–338.

Penner, E. and L.W. Gold (1971) Transfer of heaving forces by adfreezing to columns and foundation walls in frost-susceptible soils. *Canadian Geotechnical Journal*, 8(4): 514–526.

Penner, E. and L.E. Goodrich (1983) Adfreezing stresses on steel piles, Thompson, Manitoba. In *Proceedings, 4th International Conference on Per-mafrost, 17–22 July, Fairbanks, Alaska*. Washington, D.C.: National Academy Press, p. 979–983.

Penner, E. and W.W. Irwin (1969) Adfreezing of Leda clay to anchored footings columns. *Canadian Geotechnical Journal*, 6(3): 327–337.

Péwé, T.L. (1982) Geologic hazards in the Fairbanks area, Alaska. Alaska Geological and Geophysical Surveys, Special Report 15.

Saltykov, N.I. (1944) Calculating frost heaving forces on foundations. *Izvestiia Akademia Nauk SSSR, Otdelenie Tekhnickeskikh Nauk*, No. 6: 305–412. (Library of Congress, SIPRE Bibliography Project, Translation 46.)

Sohlberg, E.T. (1965) Strain gage instrumentation of steel piles in snow. USA Cold Regions Research and Engineering Laboratory, Technical Report 152. AD 615 996.

Sutherland, H.B. and P.N. Gaskin (1973) Porewater and heaving pressures developed in partially frozen soils. In *Permafrost: North American Contribution to the Second International Conference, 13–28 July, Yakutsk, U.S.S.R.* Washington, D.C.: National Academy of Sciences, p. 409–419.

Tice, A.R., J.L. Oliphant, Y. Nakano and T.F. Jenkins (1982) Relationship between the ice and unfrozen water phases in frozen soil as determined by phased nuclear magnetic resonance and physical desorption data. USA Cold Regions Research and Engineering Laboratory, CRREL Report 82-15. ADA 118 486.

Trow, W.A. (1955) Frost action on small footings. Highway Research Board Bulletin No. 100, p. 22–27.

Tsytovich, N.A. (1975) *The Mechanics of Frozen Ground*. New York: McGraw-Hill Book Co., p. 157–162.

Yong, R.N. (1967) On the relationship between partial soil freezing and surface forces. In *Proceedings, International Conference on Low Temperature Science*, vol. II, p. 1376–1385.

Yong, R.N. and J.C. Osler (1971) Heaving and heaving pressures in frozen soils. *Canadian Geotechnical Journal*, 8(2): 272–282.

APPENDIX A: INSTRUMENTATION AND DATA REDUCTION

STRAIN MEASUREMENTS

A Hewlett-Packard (HP) 3497A data acquisition/control unit and an HP 85 computer were used to measure the static strains in both the pipe and H-piles. The strain gauges were connected into Wheatstone bridges where one or more of the resistors were active strain gauges (Fig. A1a). The unstrained voltage ratio for a Wheatstone bridge where all the resistors have a fixed value is given by

$$(V_0/V_i)_u = [R_1/(R_1+R_4)-R_2/(R_2+R_3)] \tag{A1}$$

where V_i is the excitation voltage to the bridge (5 V nominally for this experiment), V_0 is the output voltage and R_1, R_2, R_3 and R_4 are the resistances of the bridge arms. If the resistance of one of the bridge arms changes due to straining, for example, the arm $(R_4 + \Delta R_4)$, then the strained voltage ratio would be

$$(V_0/V_i)_s = [R_1/(R_1{}^sR_4+\Delta R_4)-R_2/(R_2+R_3)]. \tag{A2}$$
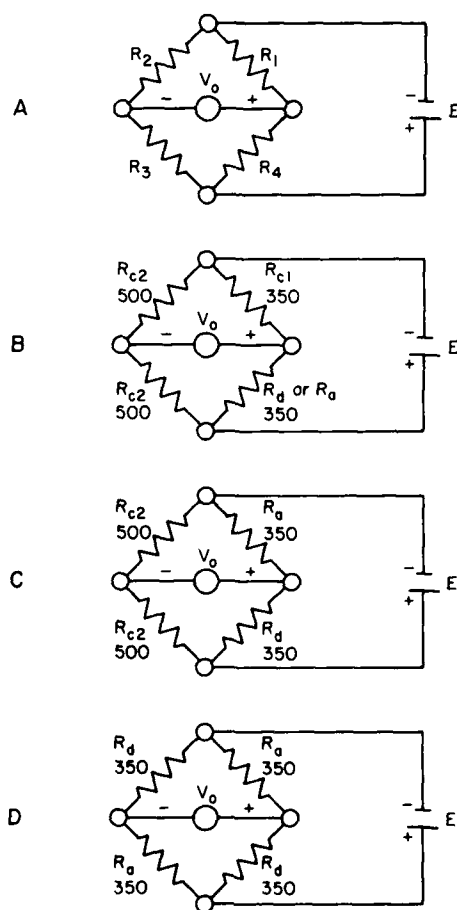

Figure A1. Wheatstone bridge circuits used to measure strain gauge resistance changes. A—general Wheatstone bridge; circuits B, C and D were used to measure one active strain gauge, uniaxial strain with temperature compensation using one active gauge, and uniaxial strain with temperature compensation using two active gauges.

35

The change in the voltage ratio between the strained and unstrained condition is given by

$$V_r = [(V_o/V_i)_s - (V_o/V_i)_u] = [R_1/(R_1 + R_4 + \Delta R_4) - R_1/(R_1 + R_4)]. \qquad \text{(A3)}$$

If $R_1 = R_4$ then

$$(-4V_r)/(1 + 2V_r) = (\Delta R_4)/(R_4). \qquad \text{(A4)}$$

The relationship between strain and changes in resistance for resistance strain gauges is

$$GF \times \epsilon = \Delta R/R$$

where ϵ is the strain and GF is the gauge factor determined by manufacturing processes. Strain is positive for positive resistance changes, which occur when the gauge is extended, and can be calculated from

$$\epsilon_4 = (-4V_r)/[GF \times (1 + 2V_r)]. \qquad \text{(A6)}$$

Equation A6 describes the situation of a Wheatstone bridge where one of the arms is an active strain gauge and the remaining arms of the bridge consist of resistors with fixed values.

In this study three different Wheatstone bridge setups were used with the strain gauges. The setup with a single active or dummy strain gauge as shown in Figure A1b was called a quarter bridge setup since three completion resistors were required to complete the Wheatstone bridge circuit. The strain for the quarter bridge setup is given by

$$\epsilon_a = (-4V_r)/[GF \times (1 + 2V_r)]. \qquad \text{(A7)}$$

Fixed-value precision resistors R_{C1} and R_{C2} shown in Figure A1b were used to complete the bridge. The precision resistors were accessed on the strain gauge multiplexer card that plugs into the back of the HP 3497A. All bridge setups were determined with reference to the bridge completion circuit in the HP 3497A.

One active strain gauge and one dummy gauge were used in a bridge setup to provide temperature compensation to the strain gauge circuit and to measure uniaxial strain (Fig. A1c). The dummy strain gauge, R_d, responds only to thermally induced apparent strains. The active strain gauge, R_a, responds to both thermally and stress-induced strains. Thus, the temperature compensated strain for one active gauge connected to a temperature compensating gauge is given by

$$\epsilon_a = (4V_r)/[GF \times (1 - 2V_r)]. \qquad \text{(A8)}$$

This bridge setup required two completion resistors to complete the circuit and was called a half bridge setup.

The final Wheatstone bridge setup consisted of two active gauges and two dummy gauges (Fig. A1d). Two of the gauges were for temperature compensation and two gauges were mounted on surfaces that were diametrically opposite from each other in the pipe pile and on opposite sides of the web for the H-pile (transverse gauges only). The resulting measurement was an average uniaxial strain given by

$$\epsilon_a = (-2V_r)/[GF \times (1 + V_r)]. \qquad \text{(A9)}$$

Since this bridge setup did not require any completion resistors in the circuit it was called a full bridge setup.

The strain at a gauge depends on the unstrained voltage ratio used in eq A3 as the reference for the strain calculations. During the field calibration tests a true unstrained common reference was determined for each strain gauge which is used to compute total strain at the gauge (App. B). The unstrained common references were determined when the upper portion of the piles were free of the surrounding soil by excavation and the piles were experiencing no load. Three local unstrained references (one for each winter data set) were also determined by inspection of the strain data and used in eq A3 to compute frost-heave-induced strains in the piles relative to the time of the local reference.

The strain gauges used to measure longitudinal strain were connected so as to reduce errors associated with temperature changes. The gauges did not exhibit any significant temperature sensitivity.

FORCE AND STRESS CALCULATIONS

After the strain measurements were obtained, the tangential forces and shear stresses acting on the piles were calculated. Several basic assumptions were used in developing the calculation scheme for forces and stresses:

1. Forces acting on the piles were due primarily to vertical shear stresses acting on the surface skin of the pile.
2. Shear stresses along the H- and pipe pile surfaces were the result of frost heaving forces or soil friction and were symmetrical in the horizontal plane.
3. The stresses acting on the piles in a horizontal plane at any given depth in the soil had azimuthal symmetry.

Figure A2 shows the force diagram for both the pipe and H-piles. A cylindrical coordinate system was used to describe the pipe pile, and a Cartesian coordinate system was used for the H-pile. Internal strains, stresses and forces in the piles are denoted by primed variables. External stresses and forces are denoted by unprimed variables.

The above assumptions imply that the stress conditions in the soil acting on the H-pile are given by

$$\sigma_x = \sigma_y, \quad \sigma_{xz} = \sigma_{yz} \tag{A10}$$

The stress–strain relationship for the pile is given by

$$\epsilon_z' = \sigma_z'/E - \nu(\sigma_x' + \sigma_y')/E \tag{A11a}$$

and

$$\epsilon_x' = \sigma_x'/E - \nu(\sigma_y' + \sigma_z')/E \tag{A11b}$$

where ϵ_z' and ϵ_x' can be determined from strain gauges mounted on the pile, Young's modulus is E, ν is Poisson's ratio for the pile and σ_x', σ_y', σ_z' are the stresses in the pile acting along the x, y and z coordinate axes. The system of equations (eq A11) is not solvable in its present form since there are only two equations and three unknowns. If, however, it is assumed that σ_y' in the vicinity of the ϵ_x' and ϵ_z' strain gauges is zero, due to the protective angle iron, then

37
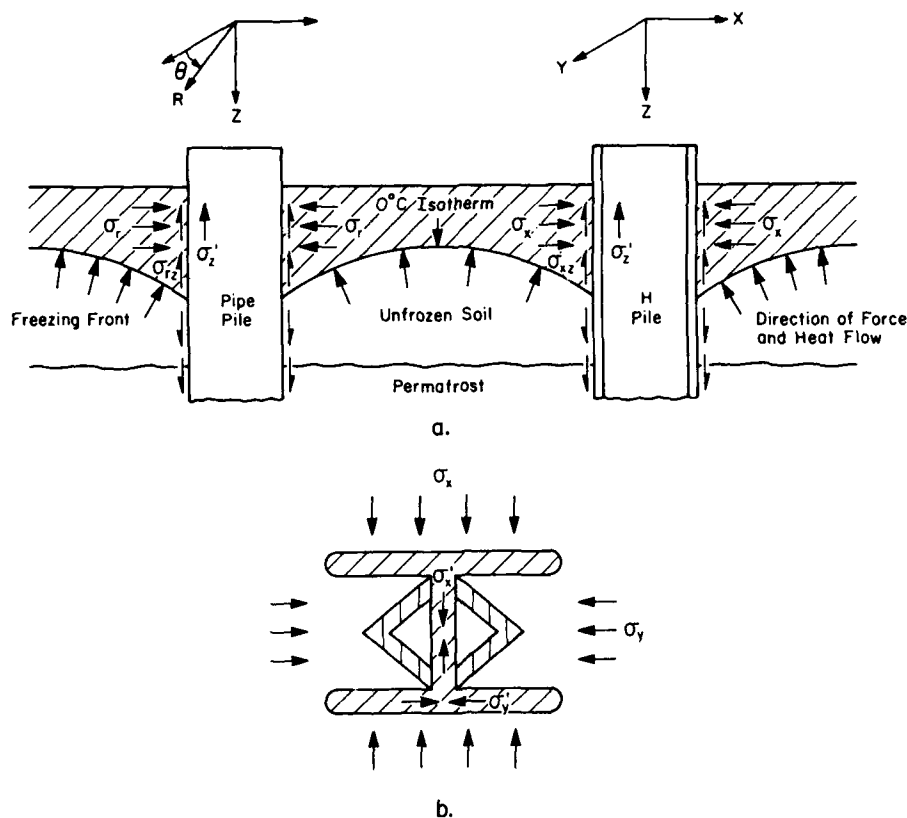
Figure A2. The direction of force and heat flow (a) and the forces acting on the H-pile in the horizontal plane using two active gauges (b).

the equations become

$$\epsilon_z' = \sigma_z'/E - (\nu\sigma_x')/E \tag{A12a}$$

$$\epsilon_x' = \sigma_x'/E - (\nu\sigma_z')/E. \tag{A12b}$$

Furthermore, the magnitude of transverse stresses, σ_x', is determined by soil confining forces acting against the pile. If these forces are small compared to σ_z', then eq A12 can be simplified. One method of estimating the magnitude of σ_x is to compare ϵ_x' to ϵ_z'. If $\sigma_x' \approx -\nu\epsilon_z'$ then the transverse strain is primarily a Poisson's ratio effect caused by σ_z', and $\sigma_x' << \sigma_z'$. This result would also imply that $\sigma_y' << \sigma_z'$, and the longitudinal stress in the pile can then by given by

$$\sigma_z' = E\epsilon_z'. \tag{A13}$$

If, however, $\epsilon_x' > -\nu\epsilon_z'$ then the longitudinal stress must be calculated using

$$\sigma_z' = E(\sigma_z' + \nu\epsilon_x')/(1 - \nu^2). \tag{A14}$$

The strain data for the 1983–84 season indicated that $\epsilon_x' \approx -\nu\epsilon_z'$, so eq A13 was used to calculate stress in the H-pile (Fig. A3).

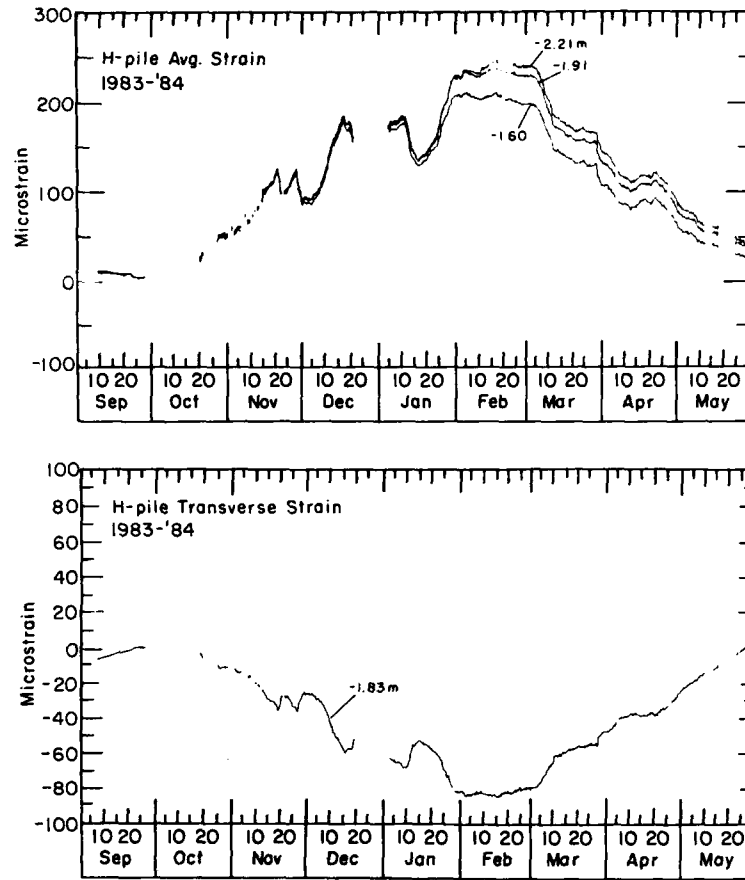*Figure A3. Average longitudinal strain for the H-pile at depths of 1.60, 1.91 and 2.21 m for the period of 1 September 1983 to 1 June 1984, and average transverse strain for the H-pile at a depth of 1.83 m for the period of 1 September 1983 to 1 June 1984.*

The internal axial force acting in the pile was determined from eq A13 by first calculating the axial force in the pile at each strain gauge depth using

$$F_z' = \sigma_z' \times CA_H = E\epsilon_z' \times CA_H. \tag{A15}$$

where CA_H is the cross-sectional area of the H-pile ($CA_H = 0.01550$ m^2). The shear stress acting on the pile was then determined from

$$\sigma_{xz} = [(F_z')_i - (F_z')_{i-1}]/(SA_H \times \Delta z) \tag{A16}$$

where $SA_H = 1.67102$ m^2, the actual surface of the H-pile per lineal meter, and Δz is the distance in meters between two adjacent strain gauge locations. Shear stresses computed on the basis of the "boxed-in" surface area of the H-pile used $SA_H = 1.02789$ m^2 per lineal meter of pile ("boxed-in" surface area = 2 [flange width + pile depth]). The force difference between two adjacent strain gauge depths is given by $[(F_z')_i - (F_z')_{i-1}]$, where the ith strain gauge location is deeper in the soil than the ith-1 location. This means that s_{xz} is positive for an upwardly directed local shear stress.

39

Calculating the shear stresses for the pipe pile was done in a similar manner as for the H-pile. The stress conditions along the pipe/soil interface are given, due to the assumptions of the problem, by

$$\sigma_r = \sigma_\theta, \text{ and } \sigma_{zr} = \sigma_{z\theta}. \tag{A17}$$

The strains for the pipe pile are given by

$$\epsilon_\theta' = (\sigma_\theta' - \nu\sigma_z')/E \tag{A18a}$$

and

$$\epsilon_z' = (\sigma_z' - \nu\sigma_\theta')/E. \tag{A18b}$$

The radial component of stress, σ_r', is zero since the strain gauges are mounted on a free surface.

Analysis of the 1982–83 winter's records indicated that, for large magnitude changes in ϵ_z', $\epsilon_\theta' \approx -\nu\epsilon_z'$. Therefore $\sigma_\theta' << \sigma_z'$ and the stress in the pipe pile was determined from

$$\sigma_z' = E\epsilon_z'. \tag{19}$$

The tangential force and shear stresses on the pile were then calculated from

$$F_x' = \sigma_z' \times CA_p \tag{A20}$$

$$\sigma_{rz} = [(F_z')_i - (F_z')_{i-1}]/(SA_p \times \Delta z) \tag{A21}$$

where $CA_p = 0.00942 \text{ m}^2$ is the cross-sectional area of the pipe pile, $SA_p = 1.01740 \text{ m}^2$ is the surface area per lineal meter of the pile and Δz is the distance in meters between adjacent strain gauges.

TEMPERATURE MEASUREMENTS

Both thermocouples and thermistors were used to measure temperatures. Thermocouple voltages were referenced against a thermocouple compensation unit built into the HP 3497A multiplexer card. The compensated voltages were converted to degrees Celsius using the HP 85 computer/controller and outputted to a storage tape. The resistance of the thermistors was measured using a 10-μA constant current source provided by the HP 3497A, which was activated only during the measurement period. The calibration of each thermistor was checked at the freezing point prior to their installation. The 0°C thermistor resistance data were then used to adjust the manufacturer's calibration curve for the thermistors. The temperature in kelvins was calculated from

$$1/T = A + B(\ln R) + C(\ln R)^3 \tag{A22}$$

where T is the temperature in kelvins and R is the thermistor resistance. A, B and C are coefficients that are calculated from the corrected calibration curve for each thermistor:

$$A = y_1 - Bx_1 - Cx_1^3 \tag{A23}$$

40

$$B = \frac{(x_1^3 - x_3^3)(y_1 - y_2) - (y_1 - y_3)(x_1^3 - x_2^3)}{(x_1 - x_2)(x_1^3 - x_3^3) - (x_1 - x_3)(x_1^3 - x_2^3)} \qquad \text{(A24)}$$

$$C = \frac{(x_1 - x_3)(y_1 - y_2) - (x_1 - x_2)(y_1 - y_3)}{(x_1 - x_3)(x_1^3 - x_2^3) - (x_1^3 - x_3^3)(x_1 - x_2)} \qquad \text{(A25)}$$

where $y_1 = 1/T$, $y_2 = 1/T_2$, $y_3 = 1/T_3$, $x_1 = \ln R_1$, $x_2 = \ln R_2$ and $x_3 = \ln R_3$.

For this study the corrected resistances R_1, R_2 and R_3 for three temperatures 273.15K, 268.15K and 263.15K were used to calculate the A, B and C coefficients for each thermistor. Equation A22 was then used to calculate soil temperatures from the thermistor data.

APPENDIX B: CALIBRATION TEST RESULTS FOR THE H- AND PIPE PILES

Both the H-pile and pipe piles were initially calibrated in compression from 0 to 44.5 kN. The initial calibration tests were conducted prior to installing the piles at the test site in order to determine an effective Young's modulus and Poisson's ratio for each strain gauge. A reaction beam loading device consisting of a 44.5-kN hydraulic cylinder, 44.5-kN calibrated load cell and loading platens constrained by four 1.9-cm-diam steel rods was used to load both the pipe-and H-piles. The instrumented section of the pipe pile was continuously supported along its 2.7-m length and the 9.0-m-long H-pile was supported every 0.3 m during the loading tests. Figure B1 shows the loading frame and data acquisition system used in the initial calibration test on the pipe pile. The initial calibration results were used until the field calibration was done in order to analyze the data during the 1982–83 and 1983–84 data collection seasons.

A concern throughout the study was the continued applicability of the initial calibration results to the analysis of the data. Several gauges were known to have been damaged during a lightning storm in the summer of 1983, and the concern was that this may have caused a calibration change in some of the undamaged gauges. Field calibration tests were conducted on 20–21 June 1985 to determine if there had been any change in the response characteristics of the gauges. The frozen ground surrounding the upper 3.7 m of the piles was thawed with steam thaw points (Fig. B2) and excavated away from the piles. The piles at depth were still frozen and anchored into the permafrost but now completely free of the surrounding soil throughout the upper instrumented section. During the soil thawing period and throughout the calibration tests the ground and pile temperatures were carefully monitored to maintain the frozen condition of the piles at depth. A tensile load was applied to the piles with a crane pulling vertically against the restraining forces holding the pile in the permafrost at depth. Both piles were carefully monitored to ensure that no vertical displacement occurred during the test loading and that the loading was truly vertical with no induced bending on the piles. The maximum tensile loads applied during the field calibration were 113 and 81 kN, respectively, on the H- and pipe piles. The limiting factor affecting the maximum load that could be applied to

the piles was the ground support beneath the crane. As the load increased, the crane's outriggers and supports were forced deeper into the ground. Both piles were incrementally loaded in tension from zero to the maximum load that could be maintained and then incrementally unloaded. A 444.8-kN calibrated load cell was used to measure the load applied by the crane. Each test load

Figure B1. Load frame and data acquisition system used in the initial compression calibration tests (pipe pile calibration).

43

Figure B2. Thawing of frozen ground around the upper 3.7 m of the H-pile using steam thaw points prior to field calibration.

was carefully monitored and the data rejected if the load varied by 0.5 kN or more. Strain measurements were made using the existing instrumentation and datalogging system, which recorded outputs from both piles throughout the calibration tests. The sensor outputs from the pile not being loaded in tension represented a true no-load, unconfined and unstrained condition. The unstrained observations were averaged, tested for outliers (none found) and used as a common unstrained reference to compute total forces for comparison of all three data sets (1982–83, 1983–84 and 1984–85).

The data from both the initial compression calibration tests and from the field tension calibration tests were analyzed for comparison. Linear least-squares curve fits were used to determine the relationship between strain and stress from the strain-load measurements for each longitudinal strain gauge sensor. Figures B3 and B4 show representative plots of the strain–stress data and the best-fit line with a slope of $1/E$, where E is Young's modulus. Figure B3 shows the results from a strain gauge that responded quite linearly, while B4 shows the results from a malfunctioning gauge.

The correlation coefficient for the least-squares curve fit to the data from the malfunctioning gauge was fairly high. It is apparent, however, from the data point distribution that the gauge response was not reliable. Therefo. ?, only data sets with correlation coefficients greater than $r = 0.95$ were accepted as functioning. The strain–stress response was also checked by examining the data plots for each gauge and through residual analyses of the data for each gauge.

A comparison was made between the averaged longitudinal gauge responses for both the initial and field calibration tests on the H-pile. Figure B5 shows the results from the initial (compression) calibration test and Figure B6 shows the results from the field (tension) calibration test. Only the good longitudinal gauges (with correlation coefficients greater than 0.95) were used to determine the averaged longitudinal gauge responses. The initial calibration test showed a loading sequence effect (Fig. B5b) that was determined to be caused by frictional losses between the pile and the required supports when the pile was tested on its side during the compression test. The initial calibration also showed a non-constancy of error variance
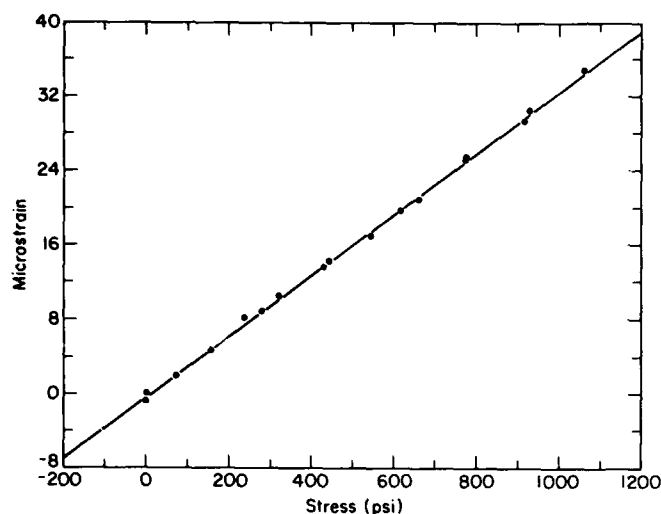
44

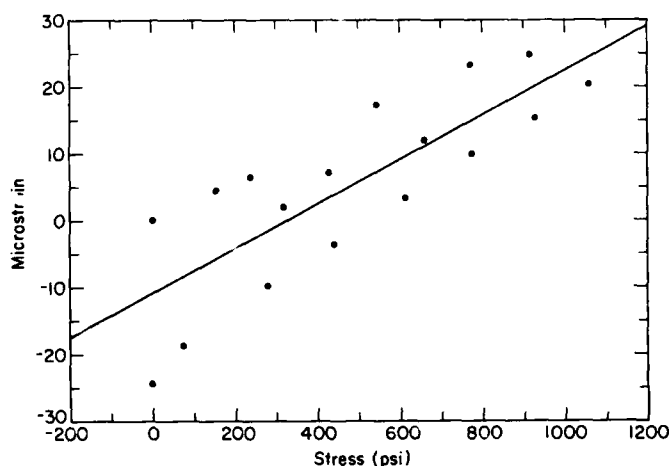Figure B3. Strain–stress curve for strain gauge 21 on the H-pile with correlation coefficient r = 1.00.

Figure B4. Strain–stress curve for malfunctioning strain gauge 11 on the H-pile with correlation coefficient r = 0.81.

(Fig. B5c) indicating that the error variance is larger at the lower loads. The non-constancy of error variance problem is due to errors in determining the lower loads for measurements made at the low end of the load cells' range. The results from the field (tension) calibration test show no sequence of loading (Fig. B6b) or non-constancy of error problem (Fig. B6c). The results from both the initial and field calibration were also tested to determine if the two regression lines (Fig. B5a and B6a) were the same and could be pooled. The test indicated that the results from the initial and field calibration were different and could not be pooled. Consequently, the results of the field calibration tests were determined to be better suited to the analysis of the data and were used for all three data sets (1982–83, 1983–84 and 1984–85).

Several gauges on both piles had acceptable gauge responses during the field calibration, but their response was found to deviate relative to comparable gauges over the period of record. The

gauges that exhibited responses inconsistent with those of comparable gauges were considered bad.

Linear least-squares fits were used to determine the relationship between transverse strain and the average longitudinal strain of the "good" longitudinal gauges. Transverse gauge data sets with correlation coefficients less than –0.95 were accepted as functioning.

The field calibration results for the H-pile are summarized in Table B1. Malfunctioning gauges were indicated by footnotes. Only 15 of the 29 longitudinal gauges on the H-pile were considered usable for the final data analysis. The effective Young's modulus averaged 203.67 GPa for the 15 good longitudinal gauges. This value is only slightly lower than the published Young's modulus for steel of 206.84 GPa (30,000,000 psi). Only one out of four gauge pairs was considered usable for the transverse gauges on the H-pile. The effective Poisson's ratio of 0.35 for gauge pair 10 and 30 is only slightly higher than the 0.33 value generally
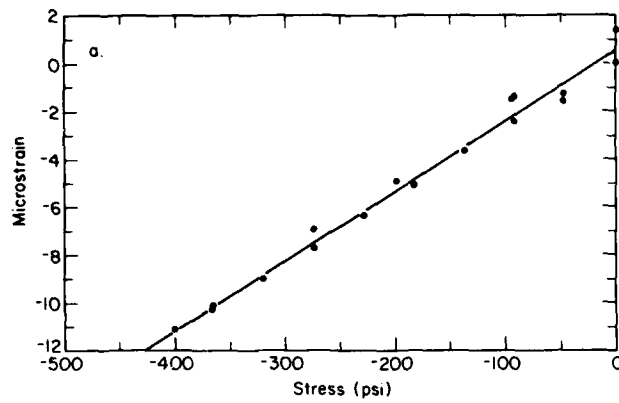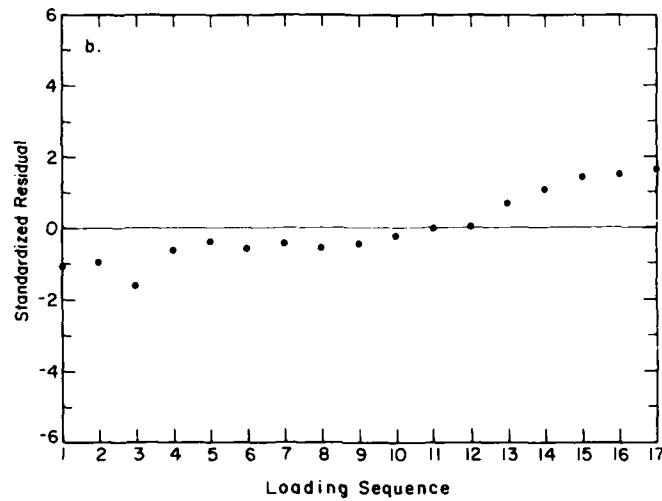
45

a. Strain-stress curve.

b. Standardized residual vs loading sequence.
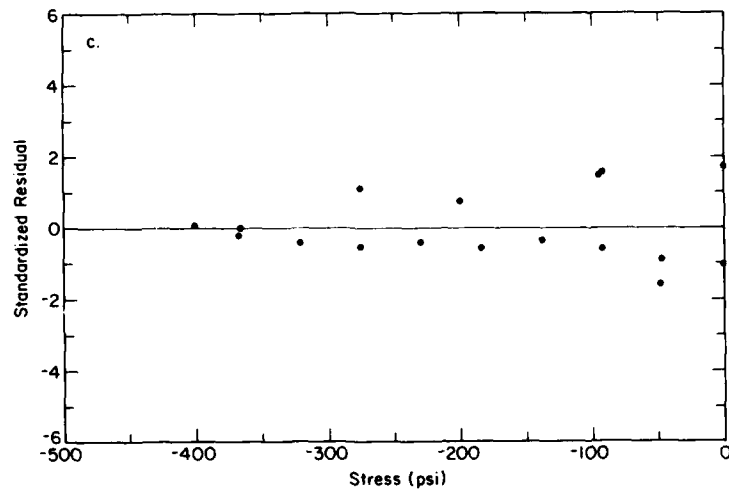
c. Standardized residual vs averaged longitudinal stress.

Figure B5. Averaged longitudinal gauge response from the initial (compression) calibration test.
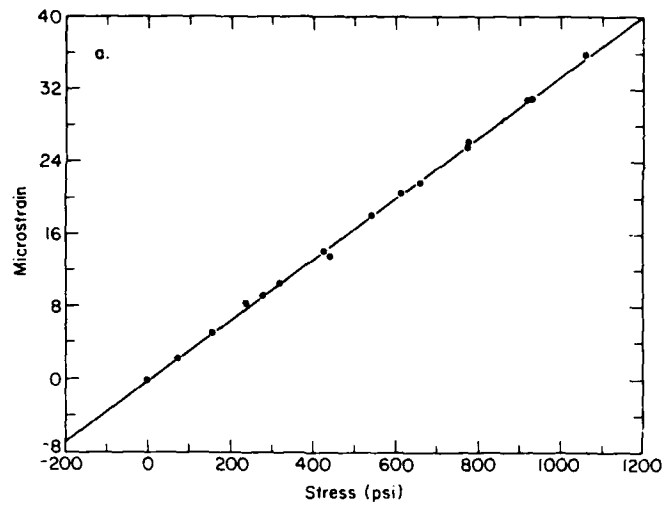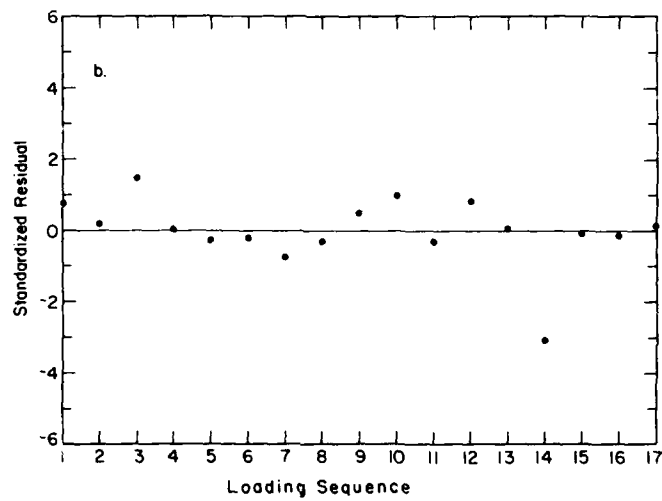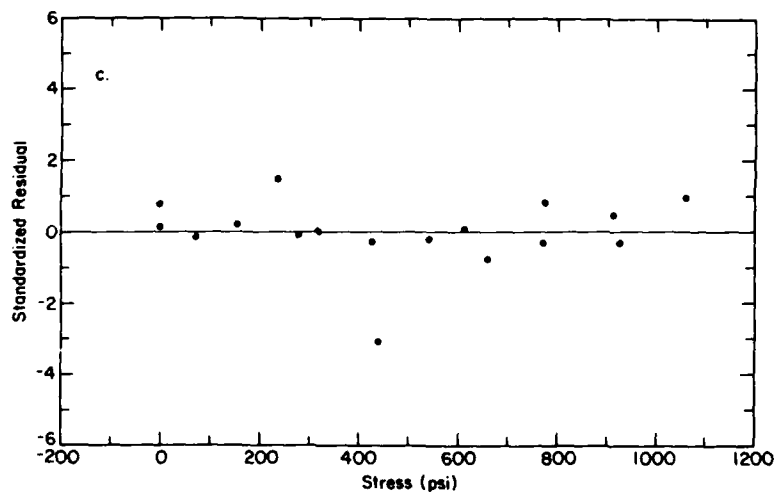
46

a. Strain-stress curve.

b. Standardized residual vs loading sequence.

c. Standardized residual vs averaged longitudinal stress.

Figure B6. Averaged longitudinal gauge response from the field (tension) calibrated test.

47

Table B1. Field calibration results for the H-pile.

Longitudinal gauges

Distance from top of pile (m)	Side one gauges			Side two gauges		
	Gauge number, completion circuit type and notes	Young's modulus (GPa)	Correlation coefficient	Gauge number, completion circuit type and notes	Young's modulus (GPa)	Correlation coefficient
0.38	1 (HB)[2]	218.65	+1.00	15 (HB)[2]	200.77	+0.97
0.53	No gauge			16 (HB)[2]	221.40	+0.99
0.69	2 (HB)[2]	221.79	+1.00	17 (HB)[2]	226.21	+0.97
0.84	No gauge			19 (HB)[2]	207.86	+0.99
0.99	4 (HB)	212.60	+0.99	20 (HB)	191.28	+1.00
1.14	No gauge			21 (HB)	209.95	+1.00
1.30	5 (HB)	212.86	+0.99	22 (HB)	195.34	+1.00
1.45	No gauge			23 (HB)	219.10	+0.99
1.60	6 (HB)	211.61	+0.99	24 (HB)	208.88	+0.96
1.75	No gauge			26 (HB)	197.49	+1.00
1.91	8 (HB)	211.55	+1.00	27 (HB)	205.29	+1.00
2.06	No gauge			28 (HB)	88.43	+0.99
2.21	9 (HB)[2]	219.83	+1.00	29 (HB)[2]	201.64	+1.00
2.36	No gauge			31 (HB)	200.41	+1.00
2.52	11 (HB)[1]	208.04	+0.81	32 (HB)[2]	200.29	+1.00
2.67	No gauge			33 (HB)	208.40	+0.97
2.82	12 (HB)[1]	0.37	+0.64	34 (HB)[2]	196.48	+1.00
2.97	No gauge			35 (HB)	181.88	+0.96
3.12	14 (HB)[1]	-12.89	-0.60	37 (HB)[2]	188.57	+1.00

Transverse gauges

Distance from top of pile (m)	Side one gauges			Side two gauges		
	Gauge number, completion circuit type and notes	Poisson's ratio	Correlation coefficient	Gauge number, completion circuit type and notes	Poisson's ratio	Correlation coefficient
0.76	3 (FB)[1]	-0.28	+0.96	18 (FB)[1]		
1.68	7 (FB)[1]	10.39	-0.73	25 (FB)[1]		
2.29	10 (FB)	0.35	-1.00	30 (FB)		
3.05	13 (FB)[1]	-212.85	+0.39	36 (FB)[1]		

Notes:

1—Gauge considered bad if correlation coefficient of curve fit was less than +0.95 for Young's modulus or greater than -0.95 for Poisson's ratio.

2—Gauge is considered bad since output from this gauge drifts relative to the other gauges over the period of record.

Completion circuit types: FB—full bridge; HB—half bridge.

accepted as the Poisson's ratio of steel. Unfortunately the upper four gauge levels on the H-pile were unusable as shown in Table B1.

The field calibration results for the pipe pile are summarized in Table B2. Malfunctioning gauges are indicated by footnotes. Several full bridge completion circuits (gauge pairs) were damaged and reconnected as half bridge circuits in July 1982 (note 3). Only 5 of the 33 longitudinal gauges on the pipe pile were considered usable for the final data analysis. The effective Young's modulus averaged 229.08 GPa for the five good longitudinal gauges. This value is 11% higher than the published Young's modulus of 206.84 GPa for steel. Only 1 out of 11 transverse gauges was considered usable for the final data analysis on the pipe pile. The effective Poisson's ratio of 0.32 for gauge number 38 is only slightly lower than the 0.33 value generally accepted as the Poisson's ratio for steel.

The importance of field calibration for the strain gauges used to determine frost heave forces is apparent from the results shown in Tables B1 and B2. The final analysis for this study used only 45.9 and 13.6 percent of the total gauges installed on the H- and pipe piles, respectively.

Table B2. Field calibration results for the pipe pile.

Longitudinal gauges

Distance from top of pile (m)	Side one gauges — Gauge number, completion circuit type and notes	Young's modulus (GPa)	Correlation coefficient	Side two gauges — Gauge number, completion circuit type and notes	Young's modulus (GPa)	Correlation coefficient
0.38	1 (FB)[1]	-1007.03	-0.94	21 (FB)[1]		
0.53	2 (FB)[3]			22 (HB)[2]	405.26	+0.97
0.69	3 (HB)[1]	364.61	+0.55	24 (FB)[3]		
0.84	5 (FB)[3]			25 (HB)[2]	278.07	+0.99
0.84				26 (QB)	260.40	+1.00
0.99	6 (FB)[3]			27 (HB)[1]	261.60	+0.45
1.14	8 (FB)[3]			29 (HB)[1]	320.96	+0.80
1.30	9 (FB)[2]	-338.02	-0.99	30 (FB)[2]		
1.45	10 (FB)[3]			31 (HB)	235.24	+0.99
1.60	11 (FB)[1]	-0.72	-0.53	32 (FB)[1]		
1.75	13 (FB)[3]			34 (HB)	211.08	+0.99
1.91	14 (FB)[2]	-342.20	-1.00	35 (FB)[2]		
2.06	15 (FB)[3]			36 (HB)[1]	214.37	+0.83
2.21	16 (FB)[3]			37 (HB)	232.33	+0.99
2.36	18 (FB)[2]	-377.98	-0.97	39 (FB)[2]		
2.52	19 (FB)[2]	-318.87	-1.00	40 (FB)[2]		
2.67	20 (FB)[3]			41 (HB)	206.35	+0.98

Transverse gauges

Distance from top of pile (m)	Side one gauges — Gauge number, completion circuit type and notes	Poisson's ratio	Correlation coefficient	Side two gauges — Gauge number, completion circuit type and notes	Poisson's ratio	Correlation coefficient
0.05	44 (QB)[1]	-2403.56	+0.41			
0.61	4 (FB)[1]	-0.03	+0.95	23 (FB)[1]		
0.84	43 (QB)[1]	0.00	-0.06			
1.07	7 (QB)[1]	0.09	-0.85	28 (QB)[1]	-0.04	+0.86
1.68	12 (FB)[1]	-0.18	+0.96	33 (FB)[1]		
1.75				42 (QB)[1]	0.02	0.32
2.29	17 (QB)[1]	0.33	-0.95	38 (QB)	0.32	-0.96

Notes:

1—Gauge considered bad if correlation coefficient of curve fit was less than +0.95 for Young's modulus or greater than -0.95 for Poisson's ratio.

2—Gauge is considered bad since output from this gauge drifts relative to the other gauges over the period of record.

3—This side of the original full bridge setup was damaged so gauge is bad. Other side reconnected as half bridge setup in July 1982.

Completion circuit types: FB—full bridge; HB—half bridge; QB—quarter bridge.

A facsimile catalog card in Library of Congress MARC format is reproduced
below.